Journal of Sound and Vibration (1998) **215**(5), 1065–1099
Article No. sv981634

THE EFFECTS OF IMPERFECTIONS ON THE PERFORMANCE OF THE SUBHARMONIC VIBRATION ABSORBER SYSTEM

C.-P. Chao and S. W. Shaw

Department of Mechanical Engineering, *Michigan State University*, *East Lansing*, *MI* 48824, *U.S.A.*

(*Received* 14 *March* 1997, *and in final form* 18 *March* 1998)

A recent study has demonstrated a new configuration of centrifugal pendulum vibration absorbers (CPVAs) that is very effective at reducing torsional vibration levels in rotating systems that are subjected to harmonic external torques. This system is composed of a pair of absorber masses riding on epicycloidal paths that are tuned to one-half order relative to the frequency of the applied torque. In the desired response, the two absorbers move in direct opposition to one another in a second-order subharmonic manner. The basic analysis of this subharmonic vibration absorber system assumes that the paths for the absorber masses can be perfectly manufactured and are exactly tuned as desired. The primary goal of this study is to explore the effects that imperfections and intentional mistuning of the absorber paths have on performance of the system. The results obtained allow one to select certain features of the path in order to achieve the desired performance, even in the face of uncertainties. To this aim, the equations of motion are first derived for a simplified model, consisting of two absorber masses and a rigid rotor. This system is shown to possess a one-to-one internal resonance subjected to two-to-one resonant external excitation. By making use of some scaling assumptions on the system parameters, the method of averaging is applied in order to obtain approximate solutions of the equations of motion. These are used to evaluate the absorber performance in terms of two performance measures: the magnitude of the rotor acceleration and the range of the disturbing torque over which the absorbers operate effectively. The results obtained are distilled into design guidelines in terms of how one should choose certain mistuning parameters for the absorber paths in order to achieve satisfactory system performance. In summary, it is determined that one should keep the two absorber paths as identical as possible, but that a small level of identical overtuning in each path will provide a certain level of robustness. In addition, it is also shown that this mistuning can be used to adjust a tradeoff between torsional vibration levels and the operating torque range for the system.

1. INTRODUCTION

Torsional vibrations in rotating systems are induced primarily by torques transmitted to a rotor from forces applied to attached components. For example, in IC engines, cylinder gas pressure and the inertia of slider-crank components cause these torques, while in helicopter rotors aerodynamic loads on blades are their primary source. These torsional vibrations can propagate through the system and cause fatigue and NVH difficulties. A centrifugal pendulum vibration absorber (CPVA) is a device used for reducing these torsional vibrations. It consists essentially of a mass that is restricted to move along a prescribed path relative to the base rotating system. The absorber is driven by the centrifugal field generated by rotation, and its motion provides a restoring torque which is designed to reduce torsional vibrations of the rotating system. An important feature of

0022–460X/98/351065 + 35 $30.00/0

the CPVA is that it can be tuned to a given multiple of the mean rotation rate, Ω. In this way, by proper geometric design of the absorber path, it can be tuned to counteract torques of frequency $n\Omega$, where n is referred to as the *order* of the disturbing torque.

CPVAs were invented for use in internal combustion engines several decades ago [1] and have been successfully employed to suppress torsional vibrations in light aircraft engines [2]. Previous analytical works [3, 4] have concentrated on analyzing the dynamics of CPVAs which use easily-manufactured circular paths for the absorber motion. By intentionally mistuning the absorber at small absorber amplitudes and/or by accounting for the system's nonlinear dynamic behavior over the entire amplitude range, improved behavior can be achieved over a larger operating envelope [5–10]. It should be noted that these absorber designs are capable of only partially counteracting the torsional vibrations that arise from a harmonic torque, even in an ideal setting [10–14]. This is due to residual vibrations generated by higher harmonics through nonlinear effects.

Recently, Lee *et al*. [15] proposed a novel absorber configuration which consists of a pair of identical absorbers riding on special paths tuned to *one-half* the order of the disturbing torque. Such a configuration is referred to as the *subharmonic absorber system*. It was shown in reference [15] that the torque generated by the periodic response of an ideal, perfectly tuned, undamped pair of subharmonic absorbers is *exactly* a pure harmonic over a wide range of amplitudes. This has significant advantages over conventional designs since it generates no higher-order harmonic torques, even when accounting for large-amplitude, nonlinear effects. Furthermore, it was also shown in reference [15] that this response is dynamically stable and still very effective when small amounts of system damping are included in the model.

The aforementioned results are based on the assumption that the absorber paths are perfectly tuned and are manufactured exactly as desired. In practice, however, due to manufacturing tolerances, wear, thermal effects, etc., the absorber paths are never perfect. The present work is an effort aimed at determining the sensitivity of the system response to such imperfections. In order to account for these effects and to predict the corresponding performance of the absorber system, an extensive analysis is conducted herein that includes various types of imperfections in the mathematical system model. Imperfections of two types are considered: uncertain (uncontrollable) and built-in (controllable). Our main goal will be to provide some guidelines regarding the use of built-in imperfections to insure good performance in the face of the uncertainties.

An evaluation of absorber performance is accomplished by evaluating two performance measures: the angular acceleration of the rotor and the range of the applied torque. The former is used to quantify the level of vibration reduction, which is desired to be as small as possible, while the latter is imposed by the size of the absorber masses, their placement, and their limited range of travel. In order to calculate these two performance measures, the system dynamic response is approximated using the method of averaging for a particular scaling of the system parameters. The solutions of the averaged equations are derived and considered in light of the system performance goals. Bifurcation diagrams are used to evaluate absorber performance and to distill some guidelines for the design of absorber paths.

The paper is organized as follows. In section 2 the mathematical model is derived and the imperfections are defined. In section 3 the equations of motion are massaged into a form amenable to asymptotic analysis. In section 4 averaging is performed. In section 5 approximate steady-state solutions of the averaged equations are derived based on some assumptions about the types and magnitudes of various types of imperfections. The range of validity for each type of solution is also discussed, as many solutions found from the mathematical model are nonphysical due to the limits of the absorbers' motions. In section

6 the desired solution is described, the attendant absorber performance is assessed, and some design guidelines are offered. Results of a simulation study are also presented in order to verify the analysis. In section 7 some conclusions and directions for future work are given.

2. THE MATHEMATICAL MODEL

2.1. ASSUMPTIONS

The equations of motion are derived for an idealized model that consists of a rigid rotor spinning about a fixed axis, subjected to an applied torque, and fitted with N general-path point-mass absorbers. The system is shown schematically by the cross sectional view of the rotor in Figure 1. This dynamical system consists of a rotor of moment of inertia I_d with respect to the center of rotation, denoted by O, and N absorbers moving freely on prescribed paths relative to the rotor. Each individual absorber, denoted by subscript i for the ith absorber, is considered to be a point mass with mass m_i.† The path for each absorber is specified by the function $R_i = R_i(S_i)$, where R_i is the distance from the C.G. of the absorber to point O, and S_i is an arc-length variable along the path defined relative to the frame of reference that rotates with the rotor. The origin of each S_i is the point where R_i reaches its maximum value, denoted by $R_{i0} = R_i(0)$. The nominal moment of inertia with respect to O for each absorber is defined by $I_i = m_i R_{i0}^2$. Typical paths are designed to be symmetric with respect to $S_i = 0$; i.e. $R_i(S_i) = R_i(-S_i)$. The resistance between the ith absorber and the rotor is modelled as an equivalent viscous damping with coefficient c_{ai}. Similarly, resistance between the rotor and ground is also modelled as equivalent linear viscous damping with coefficient c_0.

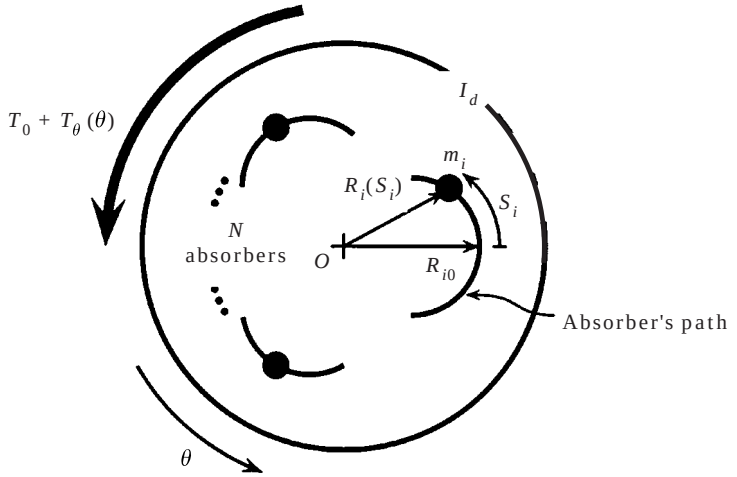

Figure 1. Cross-sectional schematic diagram of the rotor and absorbers: I_d = moment of inertia of rotor, m_2 = absorber mass, S_i = arc variable.

† It is assumed that the absorbers are physically suspended in a bifilar arrangement [2]. In this case one can account for the moments of inertia of the absorbers about their respective C.G.s by simply including them in I_d, since they rotate identically with the rotor. However, the rollers used in such configurations do not follow the rotor, an effect considered in reference [7], but not accounted for in the present study.

Let θ denote the angular displacement of the rotor. The net applied torque (including load torques) is assumed to be a nominal constant, T_0, plus a disturbing torque $T_\theta(\theta)$ which is periodic in θ. These torques arise from a variety of sources and are generally periodic with several harmonics. They may also depend on $\dot{\theta}$ and $\ddot{\theta}$. Here a simple, single harmonic model for the applied torque is considered, as there is typically a dominant harmonic and the absorber system will be designed to address it. Thus, the disturbing torque is assumed to be of order n, as follows, $T_\theta(\theta) = \hat{T}_\theta \sin(n\theta)$, where $\hat{T}_\theta > 0$. (This leaves open the potentionally large issue of nonlinear resonances that may arise from other harmonics in the excitation. This is left for future work, but see reference [12] for some results along such lines.)

2.2. EQUATIONS OF MOTION

With these assumptions, the overall system kinetic energy can be formulated. Assuming that gravitational effects are small compared to rotational effects and that the corresponding potential energy is negligible, the governing equations of motion are determined by applying Lagrange's method to the kinetic energy and including the generalized forces associated with the damping forces and the applied torque. A nondimensionalization and a change of independent variable are performed on the equations of motion for simplification. To facilitate this process, the nominal steady-state rotational speed of the rotor, Ω, is taken to be the speed at which the constant torque T_0 balances the mean component of the torque which arises from rotational damping and load; thus,

$$\Omega = T_0/c_0. \tag{1}$$

Also, a new dimensionless dependent variable y, representing the rotor speed, is introduced as

$$y \equiv \dot{\theta}/\Omega. \tag{2}$$

Then, assuming that θ is a smooth and invertible function of t, the resulting equations of motion can be transformed into a set of periodically forced, non-autonomous equations with the independent variable θ replacing t. This step transforms the nonlinearity, $\hat{T}_\theta \sin(n\theta)$, into a periodic forcing term.

The resulting dynamical system that describes the dynamics of the N absorbers and the rotor is

$$ys_i'' + [s_i' + g_i(s_i)]y' - \frac{1}{2}\frac{\mathrm{d}x_i}{\mathrm{d}s_i}(s_i)y = -\hat{\mu}_{ai}s_i', \qquad 1 \leqslant i \leqslant N, \tag{3a}$$

$$\sum_{i=1}^{N} b_i\left[\frac{\mathrm{d}x_i}{\mathrm{d}s_i}s_i'y^2 + x_i(s_i)yy' + g_i(s_i)s_i'yy' + g_i(s_i)s_i''y^2 + \frac{\mathrm{d}g_i(s_i)}{\mathrm{d}s_i}s_i'^2y^2\right]$$

$$+ yy' = \sum_{i=1}^{N} b_i\hat{\mu}_{ai}g_i(s_i)s_i'y - \hat{\mu}_0 y + \Gamma_0 + \hat{\Gamma}_\theta \sin(n\theta), \tag{3b}$$

where $(\,\cdot\,)'$ denotes $\mathrm{d}(\,\cdot\,)/\mathrm{d}\theta$, $s_i = S_i/R_{i0}$, $b_i = I_i/I_d$, $\hat{\mu}_{ai} = c_{ai}/m_i\Omega$, $\hat{\mu}_0 = c_0/I_d\Omega$, $\Gamma_0 = T_0/I_d\Omega^2$, $\hat{\Gamma}_\theta = \hat{T}_\theta/I_d\Omega^2$, and

$$x_i(s_i) = \frac{R_i^2(R_{i0}s_i)}{R_{i0}^2} \qquad \text{and} \qquad g_i(s_i) = \sqrt{x_i(s_i) - \frac{1}{4}\left(\frac{\mathrm{d}x_i}{\mathrm{d}s_i}(s_i)\right)^2} \tag{4}$$

are functions set by the path of the absorber C.G. Note that in terms of these dimensionless quantities the steady rotation condition (1) becomes

$$\Gamma_0 = \hat{\mu}_0. \tag{5}$$

2.3. THE SUBHARMONIC ABSORBER SYSTEM

2.3.1. *The perfectly-tuned absorber system*

The subharmonic absorber system proposed by Lee *et al*. [15] is composed of a pair of identical absorbers with individual masses $m_i = m_0/2$ and identical damping coefficients $\hat{\mu}_{ai} = \hat{\mu}_a$, $i = 1, 2$. These absorbers ride on identical paths specified by

$$x_i^2(s_i) = 1 - \left(\frac{n}{2}\right)^2 s_i^2, \qquad i = 1, 2 \tag{6}$$

which is equivalent to $R_i(S_i) = \sqrt{R_0^2 - (n/2)^2 S_i^2}$. This path can be shown to be a particular epicycloid [7], resulting in absorbers whose frequency of oscillation in the constant rotation rate case is $n\Omega/2$, i.e. one-half that of the applied torque. Furthermore, this frequency exactly maintains for all amplitudes up to a maximum level (described in detail below).

The equations of motion (3a) and (3b) for $N = 2$ and the identical paths given by equation (6) have an exact solution when the absorber damping is zero, $\hat{\mu}_a = 0$, and condition (5) is satisfied. It is given by

$$y(\theta) = 1, \qquad s_1(\theta) = -s_2(\theta) = \pm\frac{2}{n}\sqrt{\frac{2\hat{\Gamma}_\theta}{\nu n}}\cos\left(\frac{n}{2}\theta\right), \tag{7a, b}$$

where $\nu = (m_0 R_0^2)/I_d$ is the ratio of the total nominal moment inertia of both absorbers about point O to that of the rotor (typically $\nu \ll 1$). It is seen from equations (7a) and (7b) that in this response the rotor runs at a constant speed and the absorbers move in an exactly out-of-phase ($s_1 = -s_2$) subharmonic response of order two relative to the disturbing torque; hence the designation of the subharmonic absorber system. In this response the absorbers *exactly* counteract the applied torque over a finite range of amplitudes. The physics of this absorber response can be seen by observing equation (3b), which describes the balance of the torques acting on the rotor. It can be shown that the motions of the individual absorbers generate torque harmonics of all odd multiples of $n/2$ which, due to their out-of-phase nature, cancel each other in the summation. However, each absorber also generates, through the Coriolis term $(\mathrm{d}x_i/\mathrm{d}s_i)s_i' y^2$, an even-order torque consisting of a single harmonic of order n. In the summation these torques add together, resulting in a total absorber torque that exactly cancels the harmonic disturbing torque. This results in zero net torque acting on the rotor.

This steady-state operating condition corresponds to a perfectly constant rotor speed, which is the ultimate goal of such an absorber system. Note also that this solution, while not absolutely global, is valid and exact over a wide range of torque amplitudes (described in more detail below). When the system possesses small, non-zero absorber damping, it was shown in reference [15] that this pair of subharmonic absorbers is able to limit the rotor acceleration $\ddot{\theta}$ to a constant level that is of the same order as the absorber damping, and that this acceleration saturates at a fixed, small level as the torque amplitude is increased over a wide range.

2.3.2. *Absorber imperfections, mistuning and limitations*

The dynamically favorable property described in the previous section can only be approximated in practice. Several effects come into play that limit the ideal solution, including tolerances in the cutting process used for generating the absorber paths, the presence of rollers in the bifilar configuration (whose dynamics do not follow the absorbers' motions [7]), and deformations due to wear, elasticity and/or thermal effects. In order to account for imperfections, the absorber path functions (6) are generalized to

$$x_i(s_i, \hat{\delta}_{ij}) = 1 - \left(\frac{n}{2}\right)^2 s_i^2 - \sum_j \hat{\delta}_{ij} s_i^j, \qquad i = 1, 2, \tag{8}$$

where all $\hat{\delta}$s are assumed to be small in magnitude in the following analysis. Note that these variations contain both uncertain and built-in components.

From equation (4), it should be noted that the value of the function $g_i(s_i)$ must be real for feasible absorber motions. This leads to a restriction on the amplitudes of the absorber motions. For the case when all mistunings and imperfections are small, $\hat{\delta}_{ij} \ll 1$, the aforementioned restriction is approximated by

$$s_i(\theta) < s_{\max} + \mathcal{O}(\hat{\delta}), \qquad \forall\theta \text{ and } i, \qquad \text{where } s_{\max} = \frac{4}{n\sqrt{n^2+4}}. \tag{9}$$

This restriction keeps the absorbers below the cusp points on the epicycloidal paths. This restriction also imposes a finite operating range on the disturbing torque level $\hat{\Gamma}_\theta$. For the case of perfect absorber paths it is given by

$$\hat{\Gamma}_\theta < \bar{\hat{\Gamma}}_{\theta,0} = \frac{2nv}{n^2+4}, \tag{10}$$

over which the desired system response given in equations (7) can be maintained. This peak torque level is modified by damping and imperfections in a manner that is quantified in the sequel.

2.4. MEASURES OF PERFORMANCE

Two measures will be used to quantify the effectiveness of an absorber system. The first is the amplitude of torsional oscillations of the rotor, here represented by its peak angular acceleration during steady-state operation. The nondimensionalized angular acceleration of the rotor is given by $\ddot{\theta}(t)/\Omega^2$, and is represented in terms of the variable $y(\theta)$ by $yy'(\theta)$. The first measure of absorber performance is given by the peak value (i.e. the infinity norm) of $yy'(\theta)$ during steady-state. This quantity is denoted by $\|yy'\|_{ss}$. It will be convenient to have an explicit (even if approximate) expression for this acceleration, and this is derived in the following section.

The second performance measure is the range of the applied torque amplitude over which the absorber can operate, denoted by $\bar{\hat{\Gamma}}_\theta$. This is imposed by the cusps on the absorber paths, as stated in condition (9) above. (It should be noted that in practice, the geometry of the bifilar configuration commonly used when implementing these absorbers will impose even stricter limits than those given by the cusp.)

The general aim of an absorber system is to minimize $\|yy'\|_{ss}$ over the largest possible range, $0 < \hat{\Gamma}_\theta < \bar{\hat{\Gamma}}_\theta$. It will be seen that these goals oppose one another, and the information obtained from the present study can be used to make informed judgments for the selection of path parameters. Note also that for the perfect, undamped subharmonic absorber, $\|yy'\|_{ss} = 0$ and the corresponding torque range is given by $\bar{\hat{\Gamma}}_{\theta,0}$ in equation (10).

One of the main goals of this work is to determine $\|yy'\|_{ss}$ and the generalization for condition (10) for the damped, imperfect system. These results will point out some limitations that are imposed on the subharmonic absorber system by parameter uncertainties, but it will also offer some flexibility in designing paths to achieve certain goals.

3. SCALING AND REDUCTION OF THE EQUATIONS OF MOTION

Approximate solutions are sought for the damped and imperfect system by making some scaling assumptions and employing asymptotic analysis techniques. A series approximation for the equations of motion is derived below, leading to a form that is amenable to asymptotic analysis, which is carried out in the following section.

3.1. SCALING ASSUMPTIONS

In applications the total nominal moment of inertia of all absorbers about point O is much smaller than that of the entire rotating system. This motivates the definition of the small parameter.

$$\varepsilon \equiv \nu, \tag{11}$$

the ratio of absorber inertia to rotor inertia, which is used for the asymptotic analysis. With this definition, many of the system parameters can be scaled such that the desired system behavior can be captured by asymptotic analysis. The imperfections are handled first, after which the dissipation and forcing terms are treated.

The path imperfections are scaled by

$$\hat{\delta}_{ij} = \varepsilon\tilde{\delta}_{ij} \qquad \forall j, \qquad \text{and} \qquad i = 1, 2. \tag{12}$$

Note that typical values of the $\tilde{\delta}_{ij}$s are $<1\%$, whereas ν may range from 1 to 10%. This scaling is a conservative assumption, and it is done simply in order to incorporate the effects of imperfections in the first-order analysis. It is further assumed that the nondimensional damping and excitation parameters, $\hat{\mu}_a$, $\hat{\mu}_0$, $\hat{\Gamma}_0$ and $\hat{\Gamma}_\theta$, are also small, such that they can be scaled as

$$\hat{\mu}_a = \varepsilon\tilde{\mu}_a, \qquad \hat{\mu}_0 = \varepsilon\tilde{\mu}_a, \qquad \hat{F}_0 = \varepsilon\tilde{\Gamma}_0, \qquad \text{and} \qquad \hat{\Gamma}_\theta = \varepsilon\tilde{\Gamma}_\theta. \tag{13}$$

The unperturbed system dynamics for this scaling are determined by considering equation (3b) with $\varepsilon = 0$, i.e. $\nu = 0$, which yields $y = 1$. Using this in equation (3a) with $\hat{\mu}_a = 0$ yields a linear oscillator with frequency $n/2$ for the absorber motion. Thus, the steady-state solution of the unperturbed system is simply a constant rotor speed, $y = 1$, and the absorber motion is harmonic with frequency $n/2$ and arbitrary amplitude and phase. This limiting case can be imagined as that with a very large flywheel attached to the rotor, in which the absorbers move in a harmonic manner but have no effect on the rotor, since they are essentially massless. (This is a trivial version of the ideal subharmonic absorber response wherein the absorber masses and the applied torque are both zero.) The expansions in ε capture the first-order effects of the absorber mass, imperfections, damping and applied torque in a consistent manner.

Since the rotor speed will change smoothly as the absorber mass, the applied torque, the absorber damping and the various imperfections are increased from zero, y will be smooth in ε and can be expanded as,

$$y(\theta) = 1 + \varepsilon y(\theta) + \mathcal{O}(\varepsilon^2), \tag{14}$$

where y_1 captures the speed fluctuations induced by the net interaction of the $\mathcal{O}(\varepsilon)$ effects. Note that condition (5) is assumed to maintain as ε is increased from zero, thereby keeping the mean rotational rate very close to $y = 1$.

3.2. THE ROTOR ANGULAR ACCELERATION

As mentioned above, it is convenient to have an explicit expression for the rotor acceleration, since it is a measure of the torsional vibration amplitude. This can be derived by first noting that since $\varepsilon \ll 1$ and y_1 is bounded, $y(\theta)$ oscillates about unity and is never zero. Therefore, equation (3a) can be divided through by y in order to obtain an expression for s_i'' in terms of s_i, s_i' and y. Substitution of this expression into equation (3b) and utilization of equation (4) gives an exact expression for $yy'(\theta)$. Utilizing the definition $\varepsilon \equiv v$, the scalings in equation (13) and (12), the expansion in equation (14), and condition (5), a series approximation for yy' in terms of ε can be obtained as follows:

$$yy'(\theta) = -\varepsilon\left\{\frac{1}{2}\sum_{j=1}^{2}\left(-\frac{n^2}{2}s_j s_j' - \left(\frac{n}{2}\right)^2 g^0(s_j)s_j + \frac{\mathrm{d}g^0(s_j)}{\mathrm{d}s_j}s_j'^2\right) - \tilde{\Gamma}_\theta \sin(n\theta)\right\} + \mathcal{O}(\varepsilon^2), \quad (15)$$

where

$$g^0(s_i) = g_i(s_i; \hat{\delta}_{ij} = 0) = \sqrt{1 - \left(\frac{4n^2 + n^4}{16}\right)s_i^2}, \qquad i = 1, 2.$$

The above equation, which expresses the angular acceleration in terms of the absorber motions and the applied torque, shows that the nondimensionalized rotor acceleration is of order ε, a result consistent with the known limiting case as $\varepsilon \to 0$.

3.3. THE ABSORBER DYNAMICS

The method of averaging is used in the next section to obtain approximate solutions for the dynamic response for $0 < \varepsilon \ll 1$. Some modifications of the equations of motion are carried out in order to obtain equations in the correct form for the application of averaging. First, based on the expansions in equations (14) and (15), one can see that y'/y is the same as yy' to leading order in ε. Then by dividing equation (3a) through by y, a modified equation describing the absorber dynamics is obtained, into which the ε-series approximation of y'/y is substituted. Expanding the result in terms of ε yields a set of weakly coupled, weakly nonlinear oscillators for the absorber dyamics. These oscillators, in which the dynamics of the rotor has been eliminated to first order, are

$$s_i'' + \left(\frac{n}{2}\right)^2 s_i = \varepsilon f_i(s_1, s_2, s_1', s_2', \theta) + \mathcal{O}(\varepsilon^2), \qquad i = 1, 2, \quad (16)$$

where

$$f_i(s_1, s_2, s_1', s_2', \theta) = -\tilde{\mu}_a s_i' - h_i(s_i)$$

$$+[s_i' + g^0(s_i)]\left[\frac{1}{2}\sum_{j=1}^{2}\left(-\frac{n^2}{2}s_j s_j' - \left(\frac{n}{2}\right)^2 g^0(s_j)s_j + \frac{\mathrm{d}g^0(s_j)}{\mathrm{d}s_j}s_j'^2\right) - \tilde{\Gamma}_\theta \sin(n\theta)\right],$$

$$h_i(s_i) = \frac{1}{2}\sum_j j\tilde{\delta}_{ij}s_i^{j-1}.$$

3.4. REMARKS

- These equations are weakly coupled. The weak coupling arises due to the fact that the absorbers are not directly coupled in a physical sense, but only indirectly so through the rotor, and each absorber has only a small effect on the rotor due to its small relative inertia.
- The equations of motion are also weakly nonlinear, even though the amplitude of motion of the absorbers is not restricted to be small. The weakness of the nonlinearity is due to the epicycloidal path used for the absorbers, which renders a linear equation of motion valid for all feasible absorber amplitudes when the rotor speed is constant, and to the scaling assumptions. Again, due to the smallness of the absorbers' inertias, the rotor speed is nearly constant [cf. equations (14)], rendering nearly linear equations of motion.
- This system has two degrees of freedom with a 1:1 internal resonance. In addition, the excitation is in a 2:1 resonance with respect to the absorbers, and it contains both parametric and direct components. In this regard, the system has some similarity to the vibrations of nearly-square plates as considered by Yang and Sethna [16].
- The effects of the path imperfections are present in the functions h_i, which results from the term $1/2(\mathrm{d}x_i/\mathrm{d}s_i)y$ in the equation of motion (3a).

4. THE AVERAGED EQUATIONS

In this section some standard coordinate changes are first carried out which put the equations in the desired form. Averaging is then applied, and this followed by a discussion of the system parameters which appear in the averaged equations, and by a presentation of a modified form of the equations for a special scaling of the imperfections. With these forms of the averaged equations in hand, the search for approximate steady-state solutions is carried out in the following sections, the results of which are used for performance evaluation.

4.1. THE PERIODIC STANDARD FORM

A linear coordinate transformation between absorber displacements is first used to simplify the ensuing analysis. This transformation splits the leading order system dynamics into two invariant subspaces, representing the unison motion and its complement. A subsequent transformation to amplitude/phase coordinates will render the desired form.

The first transformation is given by

$$\xi = \frac{s_1 + s_2}{2} \qquad \text{and} \qquad \eta = \frac{s_1 - s_2}{2}. \tag{17}$$

Substituting transformation (17) into equations (16) yields the following transformed equations of motion:

$$\xi'' + \left(\frac{n}{2}\right)^2 \xi = \varepsilon \hat{f}_\xi(\xi, \xi', \eta, \eta', \theta) + \mathcal{O}(\varepsilon^2),$$

$$\eta'' + \left(\frac{n}{2}\right)^2 \eta = \varepsilon \hat{f}_\eta(\xi, \xi', \eta, \eta', \theta) + \mathcal{O}(\varepsilon^2), \tag{18}$$

where

$$\hat{f}_\xi(\xi, \xi', \eta, \eta', \theta) = -\tilde{\mu}_a \xi' - \tfrac{1}{2}h_1(\xi + \eta) - \tfrac{1}{2}h_2(\xi - \eta) + [\xi' + \tfrac{1}{2}g^0(\xi + \eta) + \tfrac{1}{2}g^0(\xi - \eta)]\, Y(\xi + \eta, \xi - \eta, \theta), \tag{19a}$$

$$\hat{f}_\eta(\xi, \xi', \eta, \eta', \theta) = -\tilde{\mu}_a \eta' - \tfrac{1}{2}h_1(\xi + \eta) + \tfrac{1}{2}h_2(\xi - \eta) + [\eta' + \tfrac{1}{2}g^0(\xi + \eta) - \tfrac{1}{2}g^0(\xi - \eta)]\, Y(\xi + \eta, \xi - \eta, \theta), \tag{19b}$$

$$Y(s_1, s_2, \theta) + \frac{1}{2}\sum_{j=1}^{2}\left(-\frac{n^2}{2}s_j s_j' - \left(\frac{n}{2}\right)^2 g^0(s_j)s_j + \frac{\mathrm{d}g^0(s_j)}{\mathrm{d}s_j}s_j'^2\right) - \tilde{\Gamma}_\theta \sin(n\theta). \tag{19c}$$

Next, the coordinate transformation to polar coordinates given by

$$\xi = r_\xi \cos\left(\varphi_\xi - \frac{n\theta}{2}\right), \qquad \xi' = n r_\xi \sin\left(\varphi_\xi - \frac{n\theta}{2}\right),$$

$$\eta = r_\eta \cos\left(\varphi_\eta - \frac{n\theta}{2}\right), \qquad \eta' = n r_\eta \sin\left(\varphi_\eta - \frac{n\theta}{2}\right), \tag{20}$$

is applied. Substituting the above transformations into equations (18) yields a set of first-order differential equations which describe the dynamics of r_ξ, φ_ξ, r_η and φ_η in the periodic standard form [17], as follows:

$$r_\xi' = \frac{2\varepsilon}{n}\hat{F}_\xi(r_\xi, \varphi_\xi, r_\eta, \varphi_\eta, \theta)\sin\left(\varphi_\xi - \frac{n\theta}{2}\right) + \mathcal{O}(\varepsilon^2), \tag{21a}$$

$$r_\xi \varphi_\xi' = \frac{2\varepsilon}{n}\hat{F}_\xi(r_\xi, \varphi_\xi, r_\eta, \varphi_\eta, \theta)\cos\left(\varphi_\xi - \frac{n\theta}{2}\right) + \mathcal{O}(\varepsilon^2), \tag{21b}$$

$$r_\eta' = \frac{2\varepsilon}{n}\hat{F}_\eta(r_\xi, \varphi_\xi, r_\eta, \varphi_\eta, \theta)\sin\left(\varphi_\eta - \frac{n\theta}{2}\right) + \mathcal{O}(\varepsilon^2), \tag{21c}$$

$$r_\eta \varphi_\eta' = \frac{2\varepsilon}{n}\hat{F}_\eta(r_\xi, \varphi_\xi, r_\eta, \varphi_\eta, \theta)\cos\left(\varphi_\eta - \frac{n\theta}{2}\right) + \mathcal{O}(\varepsilon^2), \tag{21d}$$

where the functions $\hat{F}_\xi$ and $\hat{F}_\eta$ are simply $\hat{f}_\xi$ and $\hat{f}_\eta$ expressd, respectively, in terms of coordinates r_ξ, φ_ξ, r_η and φ_η, as obtained by incorporating transformation (20) into $\hat{f}_\xi$ and $\hat{f}_\eta$. Equations (21a)–(21d) are in the required form for the application of the method of averaging.

4.2. APPLICATION OF AVERAGING

Considering only the first order terms in ε in equations (21), averaging is performed in θ over one period of the excitation, $4\pi/n$. The resulting averaged equations are expressed in terms of the first-order averaged variables $\bar{r}_\xi$, $\bar{\varphi}_\xi$, $\bar{r}_\eta$ and $\bar{\varphi}_\eta$. Due to the complicated nature of the system, this process results in many terms in the form of integrals which do not yield closed-form expressions.

In order to obtain simplified, approximate estimates of the rotor acceleration and the operating torque range, it is assumed that the oscillation amplitudes of the absorbers, i.e. $\bar{r}_\xi$ and $\bar{r}_\eta$, are small and of the same order, denoted by $\mathcal{O}(\bar{r})$. The averaged equations are then expanded in terms of $\bar{r}_\xi$ and $\bar{r}_\eta$. This yields to the following set of truncated, averaged equations, where each has been expanded to the desired order, $\mathcal{O}(\bar{r}^3)$:

$$\frac{\mathrm{d}\bar{r}_\xi}{\mathrm{d}\hat{\theta}} = \frac{-1}{2}\,\tilde{\mu}_a\bar{r}_\xi - \left(\frac{\tilde{\delta}_{\eta 2}\bar{r}_\eta}{n} + \frac{3\tilde{\delta}_{\eta 4}\bar{r}_\eta^3}{2n} + \frac{3\tilde{\delta}_{\eta 4}\bar{r}_\xi^2\bar{r}_\eta}{2n}\right)\sin(\bar{\varphi}_\xi - \bar{\varphi}_\eta) + \frac{1}{4}\,\tilde{\Gamma}_\theta\bar{r}_\xi\sin 2\bar{\varphi}_\xi$$
$$+ c_{n1}\bar{r}_\xi\bar{r}_\eta^2\sin(2\bar{\varphi}_\xi - 2\bar{\varphi}_\eta) + \mathcal{O}(\bar{r}^5), \tag{22a}$$

$$\bar{r}_\xi\frac{\mathrm{d}\bar{\varphi}_\xi}{\mathrm{d}\hat{\theta}} = \left(-\frac{\tilde{\delta}_{\xi 2}}{n} - \frac{n}{4}\right)\bar{r}_\xi - \left(\frac{\tilde{\delta}_{\eta 2}\bar{r}_\eta}{n} + \frac{3\tilde{\delta}_{\eta 4}\bar{r}_\eta^3}{2n} + \frac{9\tilde{\delta}_{\eta 4}\bar{r}_\xi^2\bar{r}_\eta}{2n}\right)\cos(\bar{\varphi}_\xi - \bar{\varphi}_\eta)$$
$$+ \frac{1}{4}\,\tilde{\Gamma}_\theta\bar{r}_\xi\cos 2\bar{\varphi}_\xi + c_{n1}\bar{r}_\xi\bar{r}_\eta^2\cos(2\bar{\varphi}_\xi - 2\bar{\varphi}_\eta) + c_{n2}\bar{r}_\xi^3 + c_{n3}\bar{r}_\xi\bar{r}_\eta^2 + \mathcal{O}(\bar{r}^5), \tag{22b}$$

$$\frac{\mathrm{d}\bar{r}_\eta}{\mathrm{d}\hat{\theta}} = \frac{-1}{2}\,\tilde{\mu}_a\bar{r}_\eta - \left(\frac{\tilde{\delta}_{\eta 2}\bar{r}_\xi}{n} + \frac{3\tilde{\delta}_{\eta 4}\bar{r}_\xi^3}{2n} + \frac{3\tilde{\delta}_{\eta 4}\bar{r}_\eta^2\bar{r}_\xi}{2n}\right)\sin(\bar{\varphi}_\eta - \bar{\varphi}_\xi) + \frac{1}{4}\,\tilde{\Gamma}_\theta\bar{r}_\eta\sin 2\bar{\varphi}_\eta$$
$$+ c_{n1}\bar{r}_\eta\bar{r}_\xi^2\sin(2\bar{\varphi}_\eta - 2\bar{\varphi}_\xi) + \mathcal{O}(\bar{r}^5), \tag{22c}$$

$$\bar{r}_\eta\frac{\mathrm{d}\bar{\varphi}_\eta}{\mathrm{d}\hat{\theta}} = -\frac{\tilde{\delta}_{\xi 2}}{n}\,\bar{r}_\eta - \left(\frac{\tilde{\delta}_{\eta 2}\bar{r}_\xi}{n} + \frac{3\tilde{\delta}_{\eta 4}\bar{r}_\xi^3}{2n} + \frac{9\tilde{\delta}_{\eta 4}\bar{r}_\eta^2\bar{r}_\xi}{2n}\right)\cos(\bar{\varphi}_\eta - \bar{\varphi}_\xi) + \frac{1}{4}\,\tilde{\Gamma}_\theta\bar{r}_\eta\cos 2\bar{\varphi}_\eta$$
$$+ c_{n1}\bar{r}_\eta\bar{r}_\xi^2\cos(2\bar{\varphi}_\eta - 2\bar{\varphi}_\xi) - c_{n4}\bar{r}_\eta^3 + c_{n3}\bar{r}_\eta\bar{r}_\xi^2 + \mathcal{O}(\bar{r}^5), \tag{22d}$$

where

$$\hat{\theta} \equiv \varepsilon\theta, \qquad \tilde{\delta}_{\xi 2} = \frac{\tilde{\delta}_{12} + \tilde{\delta}_{22}}{2}, \qquad \tilde{\delta}_{\eta 2} = \frac{\tilde{\delta}_{12} - \tilde{\delta}_{22}}{2}, \qquad \tilde{\delta}_{\xi 4} = \frac{\tilde{\delta}_{14} + \tilde{\delta}_{24}}{2}, \qquad \tilde{\delta}_{\eta 4} = \frac{\tilde{\delta}_{14} - \tilde{\delta}_{24}}{2},$$
$$c_{n1} = \frac{4n^3 - n^5}{256} - \frac{3\tilde{\delta}_{\xi 4}}{2n}, \qquad c_{n2} = \frac{n^5}{128} - \frac{3\tilde{\delta}_{\xi 4}}{2n}, \qquad c_{n3} = \frac{4n^3 + n^5}{128} - \frac{3\tilde{\delta}_{\xi 4}}{2n}$$
$$\text{and} \quad c_{n4} = \frac{n^3}{32} + \frac{3\tilde{\delta}_{\xi 4}}{2n}. \tag{23}$$

These equations contain the essential dynamics that arise from the resonant structure of this system. The stationary solutions of equations (22) represent the amplitudes and phases of the periodic steady-state responses of the absorbers, as represented by the unison and opposition modal coordinates. Non-stationary steady-state solutions are represented by amplitude and phase modulated oscillations of the averaged equations.

The averaged equations (22) as derived using these polar coordinates are singular when either ξ of η is zero. Therefore, they cannot be used for determining the stability of any trivial solutions that may exist. When faced with this situation, the following transformation is employed:

$$A_\xi = \bar{r}_\xi\cos\bar{\varphi}_\xi, \qquad B_\xi = \bar{r}_\xi\sin\bar{\varphi}_\xi, \qquad A_\eta = \bar{r}_\eta\cos\bar{\varphi}_\eta, \qquad \text{and} \qquad B_\eta = \bar{r}_\eta\sin\bar{\varphi}_\eta, \tag{24}$$

which yields an equivalent set of truncated, averaged equations expressed in Cartesian coordinates. These are given in Appendix A.

4.3. SYSTEM PARAMETERS

The averaged equations (22) depend on seven dimensionless parameters: $\tilde{\mu}_a$, $\tilde{\Gamma}_\theta$, n, $\tilde{\delta}_{\xi 2}$, $\tilde{\delta}_{n2}$, $\tilde{\delta}_{\xi 4}$ and $\tilde{\delta}_{\eta 4}$.

Note that the effects of imperfections are present in the truncated averaged equations only through the second and fourth order terms as they are defined in terms of the path formulations given in equation (8). The coefficients of odd powers of s in the path formulation, that is, $\hat{\delta}_{\xi 1}$, $\hat{\delta}_{\eta 1}$, $\hat{\delta}_{\xi 3}$ and $\hat{\delta}_{\eta 3}$, do not appear in the averaged equations (22). Thus, the analysis indicates that such terms, which measure the deviation of the paths' symmetry about their vertices, have an insignificant effect on the resonant responses. As defined in equation (23), the parameters $\tilde{\delta}_{\xi 2}$ and $\tilde{\delta}_{\eta 2}$ are the sum and difference of $\tilde{\delta}_{12}$ and $\tilde{\delta}_{22}$, respectively, and these result from the net effects of linear frequency imperfections in the dynamics of each absorber. The parameters $\tilde{\delta}_{\xi 4}$ and $\tilde{\delta}_{\eta 4}$ result from fourth-order imperfections in the absorber path realization, i.e. they capture the leading-order nonlinear imperfections that are symmetric about the path vertex.

Of the other system parameters, $\tilde{\mu}_a$ is the absorber damping which, in practice, is designed to be small and will be regarded as fixed in the following bifurcation analysis. $\tilde{\Gamma}_\theta$ is the amplitude of the disturbing torque, and this is used as the primary bifurcation parameter. Since the absorber motions are prevented from reaching the cusps on their paths, the applicable range for $\tilde{\Gamma}_\theta$ is finite for each steady-state solution branch of the averaged equations (22). The value of n is fixed by the loading condition (e.g. in an N-cylinder, four-stroke internal combustion engine, $n = N/2$). Note that the value of n affects the signs of the c_ns, and can even render them zero if $\tilde{\delta}_{\xi 4} = 0$. These differences can result in qualitatively different bifurcation diagrams, as shown below.

The term $-n\bar{r}_\xi/4$ in equation (22b), which results from expansion of the term $(n/2)^2 g(s_i)s_i$ in the ε-order function Y in equation (19c), is of particular interest. This term characterizes the difference between the linear frequencies of the two modes, i.e. $-n\bar{r}_\xi/4$ plays the role of *internal mistuning* on the system dynamics. When this term is nonzero, the perturbed system dynamics are not invariant under the exchange of the two modes. It is subsequently shown that this term plays a key role in obtaining the desired performance of the subharmonic absorber system.

4.4. AVERAGED EQUATIONS FOR NEARLY IDENTICAL ABSORBER PATHS

In order to evaluate absorber performance in terms of the two performance measures defined above, the steady-state solutions of the truncated averaged equations (22) must be determined. However, due to the complexity of the expanded averaged equations (22), it is impossible to find (even approximate) steady-state solutions in closed form. A certain class of approximate solutions can be found by employing the following, additional scaling assumption on the mistuning parameters: it is assumed that the absorbers are designed in such a manner that they are nearly identical. The motivation behind such an assumption is that one can intentionally add such imperfections in the manufacturing process in a controlled manner so that these dominate the smaller, uncontrollable imperfections, and such variations will be identical to both absorber paths.

This assumption leads to the following scaling of the imperfection parameters:

$$\frac{\tilde{\delta}_{\eta i}}{\tilde{\delta}_{\xi i}} = \mathcal{O}(\varepsilon) \qquad \text{for} \qquad i = 1, 2, \ldots . \tag{25}$$

Note that these imperfections include an intentional mistuning of the absorbers' natural frequency relative to the order of the applied torque. With scaling (25) adopted, the terms involving the $\tilde{\delta}_\eta$s in the averaged equations in equations (22) are pushed out to $\mathcal{O}(\varepsilon^2)$, and

thus have no influence on the dynamics at this level of approximation. This scaling assumption will be revisited near the end of the paper.

The resulting modified, truncated averaged equations are given by

$$\frac{\mathrm{d}\bar{r}_\xi}{\mathrm{d}\hat{\theta}} = \frac{-1}{2}\,\tilde{\mu}_a \bar{r}_\xi + \frac{1}{4}\,\tilde{\Gamma}_\theta \bar{r}_\xi \sin 2\bar{\varphi}_\xi - c_{n1}\bar{r}_\xi \bar{r}_\eta^2 \sin(2\bar{\varphi}_\xi - 2\bar{\varphi}_\eta), \tag{26a}$$

$$\bar{r}_\xi \frac{\mathrm{d}\bar{\varphi}_\xi}{\mathrm{d}\hat{\theta}} = \left(\frac{-\tilde{\delta}_{\xi 2}}{n} - \frac{n}{4}\right)\bar{r}_\xi + \frac{1}{4}\,\tilde{\Gamma}_\theta \bar{r}_\xi \cos 2\bar{\varphi}_\xi + c_{n1}\bar{r}_\xi \bar{r}_\eta^2 \cos(2\bar{\varphi}_\xi - 2\bar{\varphi}_\eta) + c_{n2}\bar{r}_\xi^3 + c_{n3}\bar{r}_\xi \bar{r}_\eta^2, \tag{26b}$$

$$\frac{\mathrm{d}\bar{r}_\eta}{\mathrm{d}\hat{\theta}} = \frac{-1}{2}\,\tilde{\mu}_a \bar{r}_\eta + \frac{1}{4}\,\tilde{\Gamma}_\theta \bar{r}_\eta \sin 2\bar{\varphi}_\eta - c_{n1}\bar{r}_\eta \bar{r}_\xi^2 \sin(2\bar{\varphi}_\eta - 2\bar{\varphi}_\xi), \tag{26c}$$

$$\bar{r}_\eta \frac{\mathrm{d}\bar{\varphi}_\eta}{\mathrm{d}\hat{\theta}} = \frac{-\tilde{\delta}_{\xi 2}}{n}\,\bar{r}_\eta + \frac{1}{4}\,\tilde{\Gamma}_\theta \bar{r}_\eta \cos 2\bar{\varphi}_\eta + c_{n1}\bar{r}_\eta \bar{r}_\xi^2 \cos(2\bar{\varphi}_\eta - 2\bar{\varphi}_\xi) - c_{n4}\bar{r}_\eta^3 + c_{n3}\bar{r}_\eta \bar{r}_\xi^2, \tag{26d}$$

where $\hat{\theta}$, c_{n1}, c_{n2}, c_{n3} and c_{n4} are the same as defined in equations (23). Utilizing transformation (24), the corresponding averaged equations (26) in term of Cartesian coordinates are determined, and these are given by equations (A2a)–(A2d) in Appendix A.

It is seen from equations (26) that in this case $\tilde{\Gamma}_\theta$, n, $\tilde{\delta}_{\xi 2}$ and $\tilde{\delta}_{\xi 4}$ are the important parameters to be considered in the bifurcation analysis. $\tilde{\delta}_{\xi 2}$ enters the averaged equations as a linear frequency detuning, while $\tilde{\delta}_{\xi 4}$ affects the coefficients of the first-order nonlinear terms. If $\tilde{\delta}_{\xi 4}$ is very small, the value of n will dictate the coefficients of the nonlinear terms, thus fixing the nature of the bifurcation diagram.

It is interesting to point out that the truncated, averaged equations (26) have the same structure as those analyzed by Yang and Sethna [16] in a study of the flexural vibrations of nearly square plates subjected to parametric in-plane excitation. In that study, two detuning parameters with respect to the natural frequencies of each individual oscillator were considered as the primary bifurcation parameters. Here, in addition to the imperfection and mistuning parameters, the disturbing torque level $\tilde{\Gamma}_\theta$ is considered as a primary bifurcation parameter in order to evaluate the system performance under various levels of the disturbing torque. For other related works on bifurcation analysis for dynamical systems composed of weakly-coupled oscillators and subject to internal and/or external resonances, see Bajaj *et al*. [18], and Ariaratnam and Sri Namachchivaya [19].

5. APPROXIMATE STEADY-STATE SOLUTIONS

This section begins with a brief discussion of the various types of steady-state responses that can occur, followed by a detailed analysis of each. Of particular interest are the existence, stability, and range of validity for these responses. The results obtained are used for the performance evaluation that follows in the next section.

5.1. SOLUTION TYPES

With assumption (25) adopted, it is evident from the averaged equations (26) that for any given system parameters there exists a trivial solution which leads to no motion of the absorbers; i.e. $\bar{r}_\xi = \bar{r}_\eta = 0$. Also, there are solutions with $\bar{r}_\xi = 0$, $\bar{r}_\eta \neq 0$ and with $\bar{r}_\eta = 0$, $\bar{r}_\xi \neq 0$. These are single-mode solutions and are denoted by "SM" in the following. Solutions with $\bar{r}_\xi \neq 0$ and $\bar{r}_\eta = 0$ are unison mode solutions, and these synchronized motions of the two absorbers are denoted as "SM1". Solutions with $\bar{r}_\xi = 0$ and $\bar{r}_\eta \neq 0$

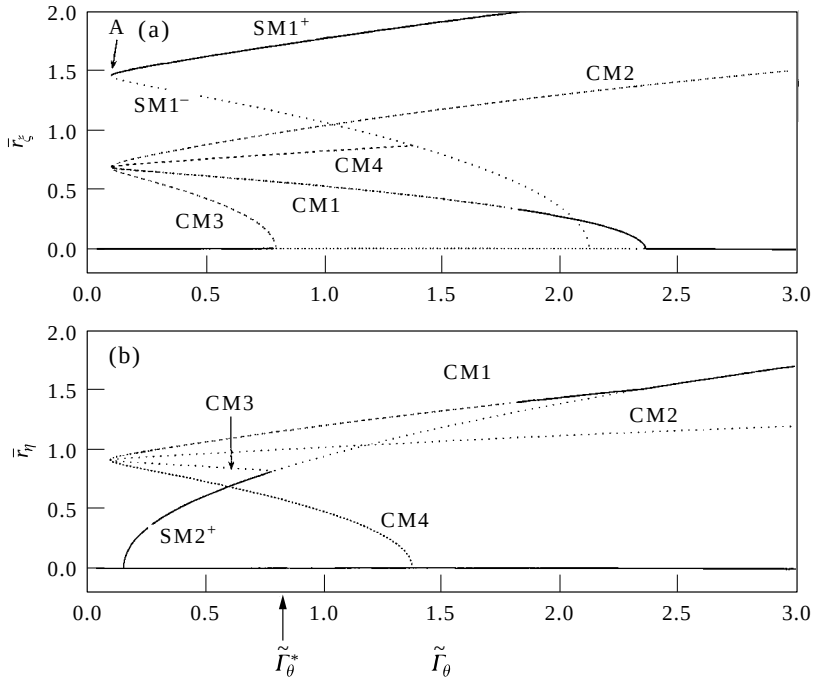

Figure 2. The bifurcation diagram for $n = 2$, $\tilde{\mu}_a = 0{\cdot}05$, $\tilde{\delta}_{\xi 2} = 0{\cdot}06$ and $\tilde{\delta}_{\xi 4} = 0$. The solid lines represent stable solutions and the dashed lines represent unstable solutions; (a) amplitudes of ξ, (b) amplitudes of η.

correspond to motions in which the two absorbers undergo oscillations with the same amplitude but are π out-of-phase, and these are denoted by "SM2". In addition, there exist coupled-mode solutions with $\bar{r}_\xi$ and $\bar{r}_\eta$ both non-zero, denoted by "CM". Note that for certain values of the system parameters, periodic solutions arising from Hopf bifurcations may exist for the averaged equations, representing amplitude and phase modulated oscillations of the absorbers. However, it will be shown that such motions are not physically possible for this system, due to the finite physical limits of the absorber paths.

As each solution type is considered, results are presented in the form of bifurcation diagrams depicted by plotting the amplitudes of the two modes versus the torque amplitude $\tilde{\Gamma}_\theta$. For this study the value of the absorber damping $\tilde{\mu}_a$ is fixed, whereas several possible values for n, $\tilde{\delta}_{\xi 2}$ and $\tilde{\delta}_{\xi 4}$ are considered. The solution branches are represented in closed form whenever possible, and are otherwise determined using numerical tools such as AUTO [20] and/or the Newton–Raphson method. Figure 2 shows a representative bifurcation diagram for the system with $n = 2$, $\tilde{\mu}_a = 0{\cdot}05$, $\tilde{\delta}_{\xi 2} = 0{\cdot}06$ and $\tilde{\delta}_{\xi 4} = 0$. This diagram is typical and depicts the general features that appear in the following analysis.

5.2. THE ZERO SOLUTION

It is evident from the averaged equations (26) that the zero solution; i.e. $\bar{r}_\xi = \bar{r}_\eta = 0$, exists for any set of system parameters. Its stability can be determined by the eigenvalues of the corresponding Jacobian matrix of equations (A2a)–(A2d) evaluated at the origin. It is found that this matrix has the form

$$J_{4\times 4} = \begin{bmatrix} A_{2\times 2} & O_{2\times 2} \\ O_{2\times 2} & B_{2\times 2} \end{bmatrix}, \tag{27}$$

where $O_{2\times 2}$ represents the two-by-two zero matrix. The eigenvalues of J thus coincide with the eigenvalues of A and B, which are

$$\lambda_{1,2} = \frac{-\tilde{\mu}_a}{2} \pm \frac{1}{4n}\sqrt{-16\tilde{\delta}_{\xi 2}^2 + \tilde{\Gamma}_\theta^2 n^2}, \qquad \lambda_{3,4} = \frac{-\tilde{\mu}_a}{2} \pm \frac{1}{4n}\sqrt{-(n^2 + 4\tilde{\delta}_{\xi 2})^2 + \tilde{\Gamma}_\theta^2 n^2}. \tag{28a, b}$$

Based on these eigenvalues, it is easy to show that for nonzero damping ($\tilde{\mu}_a \neq 0$) there are no Hopf bifurcations from the zero solution. The bifurcation sets on which an eigenvalue becomes zero are shown in Figure 3, which is depicted for the system parameters, $n = 2$ and $\tilde{\mu}_a = 0{\cdot}05$. In this figure, the zero solution is stable under the curve AOB and unstable above AOB. Note that a double zero eigenvalue condition holds at the point labelled O. All bifurcations from the zero solution are pitchfork bifurcations; super- and subcritical cases both occur, depending on the values of the system parameters.

Of course, this solution is not affected by the limitations imposed on absorber motion.

5.3. SINGLE-MODE SOLUTIONS

5.3.1. *Solution branches*

There exist two types of single-mode solutions, defined above and labelled SM1 and SM2. For SM1, the synchronous responses, the solutions with $\bar{r}_\xi \neq 0$ are determined by equations (26a) and (26b), yielding

$$\bar{r}_{\xi+}^2 = \frac{1}{4c_{n2}}\left(\frac{4\tilde{\delta}_{\xi 2}}{n} + n + \sqrt{\tilde{\Gamma}_\theta^2 - 4\tilde{\mu}_a^2}\right), \qquad \bar{r}_{\xi-}^2 = \frac{1}{4c_{n2}}\left(\frac{4\tilde{\delta}_{\xi 2}}{n} + n - \sqrt{\tilde{\Gamma}_\theta^2 - 4\tilde{\mu}_a^2}\right), \tag{29}$$

$$\tan 2\bar{\varphi}_{\xi+} = \frac{2\tilde{\mu}_a}{\sqrt{\tilde{\Gamma}_\theta^2 - 4\tilde{\mu}_a^2}}, \qquad \tan 2\bar{\varphi}_{\xi-} = \frac{-2\tilde{\mu}_a}{\sqrt{\tilde{\Gamma}_\theta^2 - 4\tilde{\mu}_a^2}}. \tag{30}$$

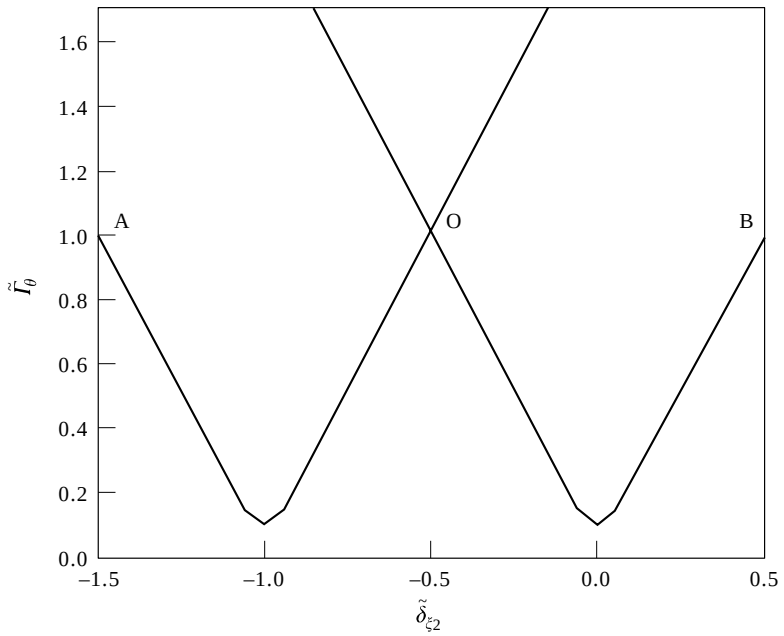

Figure 3. The bifurcation set of the zero solution for $\tilde{\delta}_{\eta 2} = \tilde{\delta}_{\eta 4} = 0$ and $\tilde{\mu}_a = 0{\cdot}05$.

The solution branches with $\bar{r}_{\xi+}$ and $\bar{r}_{\xi-}$ on SM1 are denoted by SM1$^+$ and SM1$^-$, respectively.

Utilizing the same procedure and notation, the solutions for SM2, the out-of-phase responses, are found to be

$$\bar{r}_{\eta+}^2 = \frac{1}{4c_{n4}}\left(-\frac{4\tilde{\delta}_{\xi2}}{n} + \sqrt{\tilde{\Gamma}_\theta^2 - 4\tilde{\mu}_a^2}\right), \qquad \bar{r}_{\eta-}^2 = \frac{1}{4c_{n4}}\left(-\frac{4\tilde{\delta}_{\xi2}}{n} - \sqrt{\tilde{\Gamma}_\theta^2 - 4\tilde{\mu}_a^2}\right), \tag{31}$$

$$\tan 2\bar{\varphi}_{\eta+} = \frac{2\tilde{\mu}_a}{\sqrt{\tilde{\Gamma}_\theta^2 - 4\tilde{\mu}_a^2}}, \qquad \tan 2\bar{\varphi}_{\eta-} = \frac{-2\tilde{\mu}_a}{\sqrt{\tilde{\Gamma}_\theta^2 - 4\tilde{\mu}_a^2}}. \tag{32}$$

The existence of SM1$^-$ and SM2$^-$ depend on the signs of $[(4\tilde{\delta}_{\xi2}/n) + n]$ and $[-4\tilde{\delta}_{\xi2}/n]$, respectively. Since $|\tilde{\delta}_{\xi2}| \ll 1$, it follows that $|4\tilde{\delta}_{\xi2}/n| \ll n$, and therefore SM1$^-$ always exists for the parameter ranges of interest. However, the existence of SM2$^-$ depends critically on the sign of $\tilde{\delta}_{\xi2}$. When SM1$^-$ and SM2$^-$ exist, they arise from the zero solution via pitchfork bifurcations and then merge with SM1$^+$ and SM2$^+$, respectively, in saddle-node bifurcations. If SM2$^-$ does not exist, SM2$^+$ arises directly from the zero solution through a pitchfork bifurcation. Note that the internal mistuning plays an important role in determining the nature of these single-mode solutions.

5.3.2. *Stability*

With these solutions in hand, a stability analysis is conducted by evaluating the attendant Jacobian matrix for the various single-mode solutions. It is found, as in the case for the zero solution, that the Jacobian matrix possesses the structure given in equation (27). Hence, the eigenvalues of this Jacobian matrix satisfy two second-order polynomials of the form

$$\lambda^2 + \tilde{\mu}_a\lambda + D_A = 0, \qquad \lambda^2 + \tilde{\mu}_a\lambda + D_B = 0, \tag{33}$$

derived from the block matrices A and B, respectively, in equation (27). Since $\tilde{\mu}_a > 0$, the stability of the SM1 and SM2 solutions can be determined entirely by the signs of D_A and D_B. Furthermore, due to the fact that $\tilde{\mu}_a > 0$ no Hopf bifurcations occur from SM1 or SM2. The stability for each branch on SM1 and SM2 is now determined.

Utilizing transformations (24) at zero amplitudes, D_A and D_B can be derived. For SM1,

$$D_{A1\pm} = \pm c_{n2}\bar{r}_{\xi\pm}^2\sqrt{\tilde{\Gamma}_\theta^2 - 4\tilde{\mu}_a^2}. \tag{34}$$

Since D_{A1-} is negative on the branch SM1$^-$, this leads to one positive eigenvalue, and thus SM1$^-$ is always unstable. For the branch SM1$^+$, D_{A1+} is positive and this leads to negative eigenvalues. Thus, the stability of SM1$^+$ must be determined by the sign of D_{B1+}, which is given in Appendix B. It can be shown that for $\tilde{\delta}_\xi$ small, D_{B1+} is positive. Hence, the branch SM1$^+$ is stable.

For SM2,

$$D_{B2\pm} = \pm c_{n4}\bar{r}_{\eta\pm}^2\sqrt{\tilde{\Gamma}_\theta^2 - 4\tilde{\mu}_a^2}. \tag{35}$$

Applying the same approach as that used for SM1 yields the following results: The branch SM2$^-$ is always unstable and the stability of the branch SM2$^+$ is determined by the sign of D_{A2+}, which is given in Appendix C. It can be shown that for $\tilde{\delta}_\xi$ small, D_{A2+} becomes negative at a level of $\tilde{\Gamma}_\theta$ denoted by $\tilde{\Gamma}_\theta^*$, at which point a secondary bifurcation occurs. An example of this is shown in Figure 2, where SM2$^+$ is unstable for $\tilde{\Gamma}_\theta > \tilde{\Gamma}_\theta^*$.

5.3.3. *Range of validity*

Based on condition (9), only a finite torque range is valid for each branch. (Only stable solution branches are considered here, since these will dictate the steady-state behavior.) For SM1$^+$, using equations (29) a condition can be determined such that point A in Figure 2 is above the cusp amplitude, thus violating condition (9). This condition is given by

$$\tilde{\delta}_{\xi 2} > 2nc_{n2} - (n^2/4), \tag{36}$$

which, if satisfied, implies that no stable SM1 solutions are valid. For the case with $n = 2$ and small $\tilde{\delta}_{\xi 4}$, the right-hand side of the above equation is approximately $-3/4$, and thus the condition is satisfied for any realistic value of $\tilde{\delta}_{\xi 2}$. The same argument sustains for different values of n, and it is thus concluded that for small $\tilde{\delta}_{\xi i} (i = 2, 4)$, the stable solutions on the branch SM1 do not correspond to legitimate steady-state responses for the equations of motion (3). Note that this result is largely due to the internal mistuning mentioned in section 4.2, since the term "$-n^2/4$" in the right-hand side of inequality (36) arises from the effect of internal mistuning.

On the other hand, it is seen from equations (31), representing the SM2 single-mode solutions, that internal mistuning has no effect (to leading order) on the out-of-phase responses. This allows the stable solution SM2$^+$ to be valid up to a torque level denoted by $\tilde{\bar{F}}_\theta$, at which the absorbers hit the cusps. (Note that $\tilde{\bar{F}}_\theta$, is a rescaled version of $\bar{\bar{F}}_\theta$ as defined in equation (10); i.e. $\tilde{\bar{F}}_\theta = \epsilon \bar{\bar{F}}_\theta$.) Based on the solutions given in equations (31) and the restriction on the absorber motions given by the approximation in equation (9), $\tilde{\bar{F}}_\theta$ can be approximated by

$$\tilde{\bar{F}}_\theta \simeq \left[\left(\frac{2n}{n^2 + 4} + \frac{96\tilde{\delta}_{\xi 4}}{n^3(n^2 + 4)} + \frac{4\tilde{\delta}_{\xi 2}}{n} \right)^2 + 4\tilde{\mu}_a^2 \right]^{1/2}. \tag{37}$$

This limit is now compared against the secondary bifurcation torque amplitude, $\tilde{\Gamma}_\theta^*$, described in the previous section, in order to determine which event comes first, the secondary bifurcation or the absorbers reaching the cusps. Utilizing the information given in Appendix C, the limit torque can be numerically computed and compared with equation (37). It is determined that $\tilde{\Gamma}_\theta^* > \tilde{\bar{F}}_\theta$ over the following ranges of the mistuning parameters: $\hat{\delta}_{\xi 2} \in [-0{\cdot}03, 0{\cdot}03]$ and $\hat{\delta}_{\xi 4} \in [0{\cdot}03, 0{\cdot}03]$. Therefore, the important conclusion is reached that for small imperfections the SM2$^+$ responses are stable all the way out to the cusp amplitude, and no secondary bifurcations occur. This stable SM2$^+$ branch is central to the effectiveness of the subharmonic vibration absorber system, as described in section 6.1 below.

5.4. COUPLED-MODE SOLUTIONS

The existence, stability and range of validity of the coupled-mode solutions are now considered.

5.4.1. *Solution branches and their stability*

Observing the averaged equations (26), one can first classify all possible steady-state solutions into two distinct groups: the first satisfies $\sin(2\bar{\varphi}_\xi - 2\bar{\varphi}_\eta) = 0$ and the other does not. Solutions that satisfy $\sin(2\bar{\varphi}_\xi - 2\bar{\varphi}_\eta) = 0$ are sought first. This property implies

$\cos(2\bar{\varphi}_\xi - 2\bar{\varphi}_\eta) = \pm 1$, which enables one to solve the averaged equations (26) for steady-state solutions. As a result, eight steady-state solutions are found, given by

$$\bar{r}^2_{\xi 15} = \left[\frac{c_{n4}}{4(c_{n2}c_{n4} + (c_{n3} \pm c_{n1})^2)}\right]\left[n + \frac{4\tilde{\delta}_{\xi 2}}{n} + \frac{4(c_{n3} \pm c_{n1})}{c_{n4}n}\,\tilde{\delta}_{\xi 2} + \left(\frac{-c_{n3} \mp c_{n1}}{c_{n4}} + 1\right)(\tilde{\Gamma}^2_\theta - 4\tilde{\mu}^2_a)^{1/2}\right], \tag{38a}$$

$$\bar{r}^2_{\eta 15} = \left[\frac{c_{n2}}{4(c_{n2}c_{n4} + (c_{n3} \pm c_{n1})^2)}\right]\left[\frac{-4\tilde{\delta}_{\xi 2}}{n} + \frac{(c_{n3} \pm c_{n1})}{c_{n2}}\left(n + \frac{4\tilde{\delta}_{\xi 2}}{n}\right) + \left(\frac{c_{n3} \pm c_{n1}}{c_{n2}} + 1\right)(\tilde{\Gamma}^2_\theta - 4\tilde{\mu}^2_a)^{1/2}\right], \tag{38b}$$

$$\bar{r}^2_{\xi 26} = \left[\frac{c_{n4}}{4(c_{n2}c_{n4} + (c_{n3} \pm c_{n1})^2)}\right]\left[n + \frac{4\tilde{\delta}_{\xi 2}}{n} + \frac{4(c_{n3} \pm c_{n1})}{c_{n4}n}\,\tilde{\delta}_{\xi 2} + \left(\frac{c_{n3} \pm c_{n1}}{c_{n4}} + 1\right)(\tilde{\Gamma}^2_\theta - 4\tilde{\mu}^2_a)^{1/2}\right], \tag{38c}$$

$$\bar{r}^2_{\eta 26} = \left[\frac{c_{n2}}{4(c_{n2}c_{n4} + (c_{n3} \pm c_{n1})^2)}\right]\left[\frac{-4\tilde{\delta}_{\xi 2}}{n} + \frac{(c_{n3} \pm c_{n1})}{c_{n2}}\left(n + \frac{4\tilde{\delta}_{\xi 2}}{n}\right) + \left(\frac{c_{n3} \pm c_{n1}}{c_{n2}} - 1\right)(\tilde{\Gamma}^2_\theta - 4\tilde{\mu}^2_a)^{1/2}\right], \tag{38d}$$

$$\bar{r}^2_{\xi 37} = \left[\frac{c_{n4}}{4(c_{n2}c_{n4} + (c_{n3} \pm c_{n1})^2)}\right]\left[n + \frac{4\tilde{\delta}_{\xi 2}}{n} + \frac{4(c_{n3} \pm c_{n1})}{c_{n4}n}\,\tilde{\delta}_{\xi 2} + \left(\frac{-c_{n3} \mp c_{n1}}{c_{n4}} - 1\right)(\tilde{\Gamma}^2_\theta - 4\tilde{\mu}^2_a)^{1/2}\right], \tag{38e}$$

$$\bar{r}^2_{\eta 37} = \left[\frac{c_{n2}}{4(c_{n2}c_{n4} + (c_{n3} \pm c_{n1})^2)}\right]\left[\frac{-4\tilde{\delta}_{\xi}}{n} + \frac{(c_{n3} \pm c_{n1})}{c_{n2}}\left(n + \frac{4\tilde{\delta}_{\xi 2}}{n}\right) + \left(\frac{-c_{n3} \mp c_{n1}}{c_{n2}} + 1\right)(\tilde{\Gamma}^2_\theta - 4\tilde{\mu}^2_a)^{1/2}\right], \tag{38f}$$

$$\bar{r}^2_{\xi 48} = \left[\frac{c_{n4}}{4(c_{n2}c_{n4} + (c_{n3} \pm c_{n1})^2)}\right]\left[n + \frac{4\tilde{\delta}_{\xi 2}}{n} + \frac{4(c_{n3} \pm c_{n1})}{c_{n4}n}\,\tilde{\delta}_{\xi 2}\right.$$

$$\left. + \left(\frac{c_{n3} \pm c_{n1}}{c_{n4}} - 1\right)(\tilde{\Gamma}^2_\theta - 4\tilde{\mu}^2_a)^{1/2}\right], \tag{38g}$$

$$\bar{r}^2_{\eta 48} = \left[\frac{c_{n2}}{4(c_{n2}c_{n4} + (c_{n3} \pm c_{n1})^2)}\right]\left[\frac{-4\tilde{\delta}_{\xi 2}}{n} + \frac{(c_{n3} \pm c_{n1})}{c_{n2}}\left(n + \frac{4\tilde{\delta}_{\xi 2}}{n}\right)\right.$$

$$\left. + \left(\frac{-c_{n3} \mp c_{n1}}{c_{n2}} - 1\right)(\tilde{\Gamma}^2_\theta - 4\tilde{\mu}^2_a)^{1/2}\right], \tag{38h}$$

with phases given by

$$\sin(2\bar{\varphi}_{\xi i}) = \sin(2\bar{\varphi}_{\eta i}) = 2\tilde{\mu}_a/\tilde{\Gamma}_\theta\,, \qquad 1 \leqslant i \leqslant 8. \tag{39}$$

The stability of these coupled-mode solutions can be determined by evaluating the appropriate Jacobian matrix on the corresponding solution branches and examining their eigenvalues. In this case, the characteristic equation is fourth order. Due to the complexity involved in the expressions for the stability criteria, explicit results are not given here.

The solutions in the other group, which satisfy $\sin(2\bar{\varphi}_\xi - 2\bar{\varphi}_\eta) \neq 0$, are obtained by utilizing the computational algorithm outlined in Appendix D. The corresponding stability is then determined by numerically evaluating the Jacobian matrix on the solution branches.

By comparing the single-mode and coupled solutions (denoted CM1–CM4), one finds that all coupled-mode solutions bifurcate from single-mode solution through pitchfork bifurcations. Also, no isolated coupled-mode solution branches are found to exist.

5.4.2. *Range of validity*

It is of practical importance to identify the set of stable coupled-mode solutions which satisfy condition (9), i.e. those that are physically possible. It turns out that no such solutions are valid, and this is shown by a simple argument, and backed up by detailed calculations.

First, it is known that all coupled-mode solutions bifurcate from single-mode solutions. Furthermore, in section 5.3.3. it was determined that all single-mode branches are beyond their range of validity when they undergo secondary bifurcations to coupled-mode solutions. Therefore, no coupled-mode solutions are valid for the range of parameters of interest.

A more detailed calculation follows that allows one to directly check condition (9) for all coupled-mode solutions at once over a range of parameters. To facilitate the method, a relationship between the two modal amplitudes, $\bar{r}_\xi$ and $\bar{r}_\eta$, is first derived. Setting the right-hand side of the averaged equations (26) equal to zero yields

$$0 = -2\tilde{\mu}_a + \tilde{\Gamma}_\theta \sin 2\bar{\varphi}_\xi - 4c_{n1}\bar{r}^2_\eta \sin(2\bar{\varphi}_\xi - 2\bar{\varphi}_\eta), \tag{40a}$$

$$0 = \left(\frac{-4\tilde{\delta}_{\xi 2}}{n} - n\right) + \tilde{\Gamma}_\theta \cos 2\bar{\varphi}_\xi + 4c_{n1}\bar{r}^2_\eta \cos(2\bar{\varphi}_\xi - 2\bar{\varphi}_\eta) + 4c_{n2}\bar{r}^2_\xi + 4c_{n3}\bar{r}^2_\eta, \tag{40b}$$

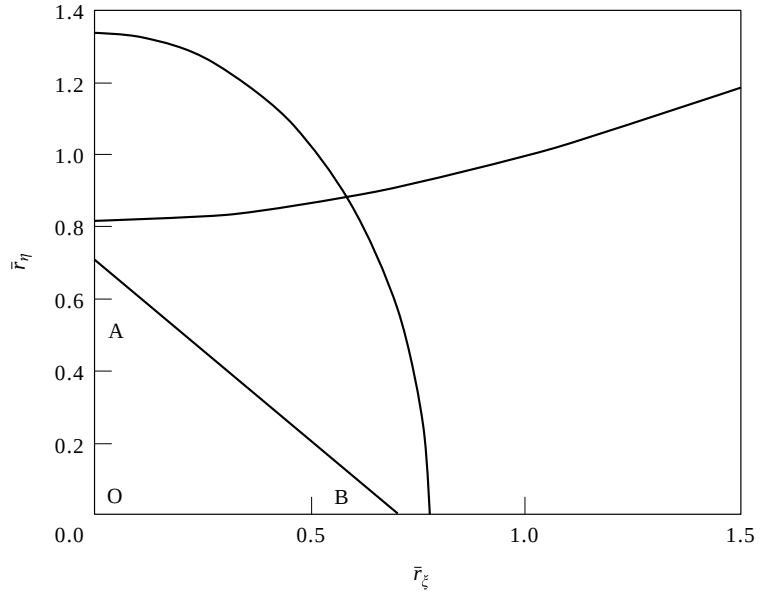

Figure 4. The relationship between $\bar{r}_\eta$ and $\bar{r}_\xi$ in coupled-mode solutions for $n = 2$, $\tilde{\delta}_{\xi 2} = 0{\cdot}05$ and $\tilde{\delta}_{\xi 4} = 0$.

$$0 = -2\tilde{\mu}_a + \tilde{\Gamma}_\theta \sin 2\bar{\varphi}_\eta - 4c_{n1}\bar{r}_\xi^2 \sin (2\bar{\varphi}_\eta - 2\bar{\varphi}_\xi), \tag{40c}$$

$$0 = \frac{-4\tilde{\delta}_{\xi 2}}{n} + \tilde{\Gamma}_\theta \cos 2\bar{\varphi}_\eta + 4c_{n1}\bar{r}_\xi^2 \cos (2\bar{\varphi}_\eta - 2\bar{\varphi}_\xi) - 4c_{n4}\bar{r}_\eta^2 + 4c_{n3}\bar{r}_\xi^2. \tag{40d}$$

Elimination of the term $\cos (2\bar{\varphi}_\eta - 2\bar{\varphi}_\xi)$ from equations (40b) and (40d) gives

$$\left(\frac{-4\tilde{\delta}_{\xi 2}}{n} - n\right)\bar{r}_\xi^2 + \frac{4\tilde{\delta}_{\xi 2}}{n}\bar{r}_\eta^2 - \tilde{\Gamma}_\theta(\bar{r}_\eta^2 \cos 2\bar{\varphi}_\eta - \bar{r}_\xi^2 \cos 2\bar{\varphi}_\xi) + 4c_{n2}\bar{r}_\xi^4 + 4c_{n4}\bar{r}_\eta^4 = 0. \tag{41}$$

Next, incorporating equations (40a) and (40c) into equations (40b) and (40d), respectively, one can represent $\cos 2\bar{\varphi}_\xi$ and $\cos 2\bar{\varphi}_\eta$ as functions of $\tilde{\Gamma}_\theta$, $\tilde{\mu}_a$, $\tilde{\delta}_{\xi 2}$, n, $\bar{r}_\xi^2$ and $\bar{r}_\eta^2$, as follows:

$$\cos 2\bar{\varphi}_\xi = \frac{-1}{8c_{n1}\tilde{\Gamma}_\theta \bar{r}_\xi^2}\left[\tilde{\Gamma}_\theta^2 + 16c_{n1}^2\bar{r}_\xi^4 - 4\tilde{\mu}_a^2 - \left(\frac{4\tilde{\delta}_{\xi 2}}{n} + 4c_{n4}\bar{r}_\eta^2 - 4c_{n3}\bar{r}_\xi^2\right)^2\right], \tag{42a}$$

$$\cos 2\bar{\varphi}_\eta = \frac{-1}{8c_{n1}\tilde{\Gamma}_\theta \bar{r}_\eta^2}\left[\tilde{\Gamma}_\theta^2 + 16c_{n1}^2\bar{r}_\eta^4 - 4\tilde{\mu}_a^2 - \left(\frac{4\tilde{\delta}_{\xi 2}}{n} + n - 4c_{n2}\bar{r}_\xi^2 - 4c_{n3}\bar{r}_\eta^2\right)^2\right]. \tag{42b}$$

Substituting the above equations into equation (41) yields the following fourth-order polynomial which governs the relationship between the two modal amplitudes on any coupled-mode, periodic, steady-state response:

$$\alpha_1\bar{r}_\xi^4 + \alpha_2\bar{r}_\eta^4 + \alpha_3\bar{r}_\xi^2\bar{r}_\eta^2 + \alpha_4\bar{r}_\xi^2 + \alpha_5\bar{r}_\eta^2 + \alpha_6 = 0, \tag{43}$$

where

$$\alpha_1 = 2c_{n1}c_{n2} - c_{n1}^2 - c_{n2}^2 + c_{n3}^2, \qquad \alpha_2 = 2c_{n1}c_{n4} + c_{n1}^2 - c_{n3}^2 + c_{n4}^2,$$

$$\alpha_3 = -2(c_{n2}c_{n3} + c_{n4}c_{n3}), \quad \alpha_4 = (c_{n2} - c_{n1})\left(\frac{2\tilde{\delta}_{\xi 2}}{n} + \frac{n}{2}\right) - \frac{2\tilde{\delta}_{\xi 2}}{n}\, c_{n3},$$

$$\alpha_5 = 2(c_{n1} + c_{n3} + c_{n4})\left(\frac{\tilde{\delta}_{\xi 2}}{n}\right) + \frac{nc_{n3}}{2} \qquad \text{and} \qquad \alpha_6 = \frac{\tilde{\delta}_{\xi 2}^2}{n^2} - \left(\frac{\tilde{\delta}_{\xi 2}}{n} + \frac{n}{4}\right)^2. \tag{44}$$

Note that this polynomial does not depend on the torque amplitude $\tilde{\Gamma}_\theta$. Thus, for fixed values of n and the system parameters, this constraint represents two curves in the $\bar{r}_\xi$–$\bar{r}_\eta$ plane. An example for $n = 2$, $\tilde{\delta}_{\xi 2} = 0{\cdot}05$ and $\tilde{\delta}_{\xi 4} = 0$ is shown in Figure 4. Also shown in this figure is the set of amplitudes that satisfy condition (9), represented by the interior of the triangle OAB. It is seen that all points on the two curves generated by the polynomial (43) are outside the triangle OAB. Thus, no coupled-mode solutions are physically possible for this set of parameters. One can generate such graphical information for any values of n, $\tilde{\delta}_{\xi 2}$ and $\tilde{\delta}_{\xi 4}$ in order to check the feasibility of the coupled-mode solutions.

5.5. REMARKS

Bifurcation diagrams showing the periodic steady-state responses and their stabilities can now be generated. Figure 2 shows a typical bifurcation diagram for $\tilde{\delta}_{\xi 2} = 0{\cdot}06$, $\tilde{\delta}_{\xi 4} = 0$ and $n = 2$. However, as shown above, many of the solution branches are nonphysical.

AUTO [20] was utilized to confirm the results obtained above, and consistency was found in every case checked. In addition, AUTO also found some nonphysical periodic solutions to equations (26), all of which arise from the coupled-mode solutions via Hopf bifurcations.

Based on the results obtained in this section, the followng conclusion is drawn. For reasonable ranges of the system parameters, the only viable (i.e. stable) steady-state system responses are the trivial solution and those on the branch $SM2^+$. To ensure this conclusion for a given system, one can use the criterion in equation (36) and the method provided in section 5.4.2 to confirm that $SM2^+$ is the only nontrivial, stable solution that satisfies condition (9).

When the system is undamped and the paths are perfect, the solution $SM2^+$ reduces to the idealized subharmonic absorber system response given in equations (7a) and (7b). Therefore, it is not too surprising that this solution will persist in the face of imperfections, and that it will offer good performance as a torsional vibration absorber. The details of this performance are considered next.

6. ABSORBER PERFORMANCE AND DESIGN GUIDELINES

This section contains the main results of the paper, which describe the effectiveness of the absorber system in terms of the steady-state response derived above. Considered in turn are the following: some general features of the response, mathematical expressions for the two measures of system performance, detailed descriptions of the effects of the various types of imperfections (including those ignored in the analysis) on the system response, a summary of the results in the form of design guidelines, and verification by simulations.

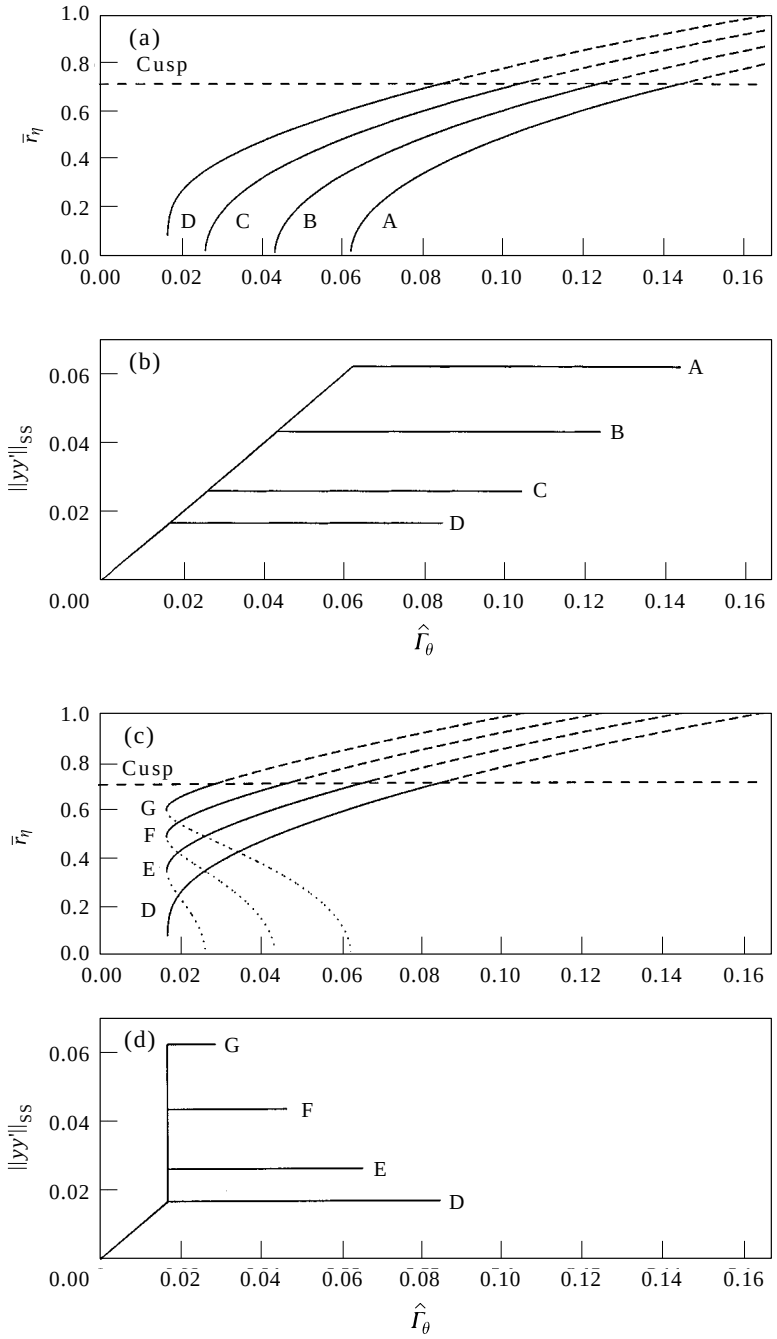

Figure 5. The response bifurcation diagram for SM2 with $n = 2$, $\hat{\delta}_{\xi 4} = 0$, $\hat{\mu}_a = 0{\cdot}0083$ and various $\hat{\delta}_{\xi 2}$. (a) $\bar{r}_\eta$ for positive $\hat{\delta}_{\xi 2}$s where $\hat{\delta}_{\xi 2} = 0{\cdot}03$, $0{\cdot}02$, $0{\cdot}01$, $0{\cdot}00$ in curves A, B, C, D, respectively; (b) rotor accelerations; (c) $\bar{r}_\eta$ for negative $\hat{\delta}_{\xi 2}$s where $\hat{\delta}_{\xi 2} = 0{\cdot}00$, $-0{\cdot}01$, $-0{\cdot}02$, $-0{\cdot}03$ in curves D, E, F, G, respectively; (d) rotor accelerations.

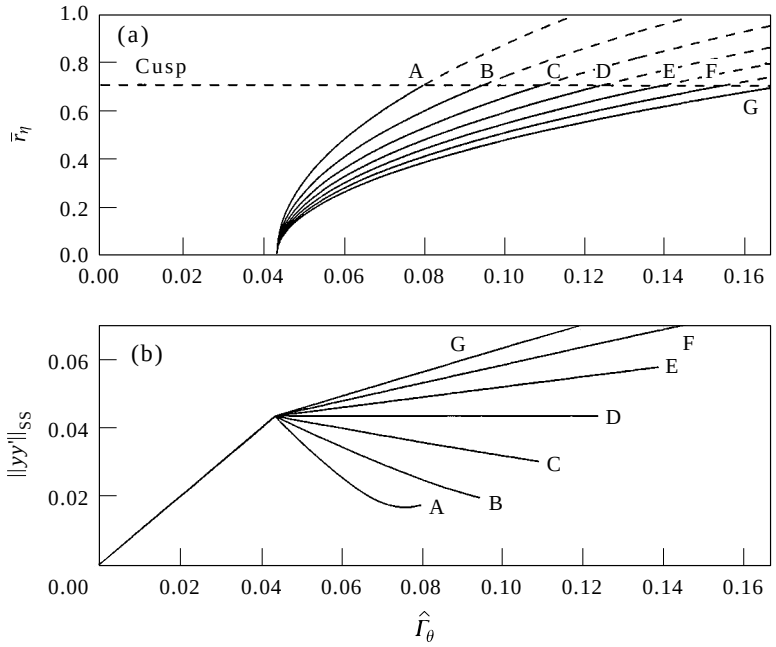

Figure 6. The response bifurcation diagram for SM2 with $n = 2$, $\hat{\delta}_{\xi 2} = 0{\cdot}02$, $\hat{\mu}_a = 0{\cdot}0083$ and various $\hat{\delta}_{\xi 4}$. (a) $\bar{r}_\eta$ for where $\hat{\delta}_{\xi 4} = 0{\cdot}03$, $0{\cdot}02$, $0{\cdot}01$, $0{\cdot}00$, $-0{\cdot}01$, $-0{\cdot}02$, $-0{\cdot}03$ in curves A, B, C, D, E, F, G, respectively; (b) rotor accelerations.

6.1. FEATURES OF THE DESIRED SOLUTION

In this section it is shown that the stable branch $SM2^+$ is very favorable in terms of meeting the two goals outlined in section 2.4.

For a given disturbing torque level $\hat{\Gamma}_\theta$, the absorber dynamics can converge to any stable steady-state solution, depending on initial conditions. Utilizing the expression for the angular acceleration yy' provided in equation (15) and the solution branches obtained by the averaged equations, one can compute the rotor acceleration on each branch. The main conclusion of these results is the following: *for various values of n, small* $\tilde{\delta}_\xi$*s and zero* $\tilde{\delta}_\eta$*, among all branches, the SM2 branches lead to the smallest* $\|yy'\|_{ss}$ *over the feasible range of the disturbing torque*.

This result can be explained in terms of the harmonics contained in yy', as follows: it is observed that the steady-state response of each absorber $s_i(\theta)$ $(i = 1, 2)$ is dominated by a harmonic term of order $n/2$ (since they are nearly linear). From this it can be determined that the net rotor acceleration yy' is generally composed of all odd harmonics, but only one even harmonic, which comes from the term $-2n^2 s_i s_j'$ in the summation. Now, suppose there is a non-zero $\bar{r}_\xi$ for the steady-state solution. In equation (15) it renders the summation of odd harmonics nonzero. Thus, these harmonics will be amplified, leading to a large value of $\|yy'\|_{ss}$. Contrarily, if $\bar{r}_\xi = 0$ for a steady-state solution, i.e. if the two absorbers simply move in an out-of-phase manner with the sample amplitude, the odd harmonics resulting from the motion of the two absorbers cancel each other in the summation, and only the even harmonic term survives. In fact, it is very close to a pure harmonic of order n, and it is precisely this effect which is used to counteract the harmonic disturbing torque, resulting in a small net angular acceleration.

Since the solution branch $SM2^+$ is desirable in terms of the rotor acceleration, it is useful to ensure that it is the only possible stable steady-state response. For a given set or range of parameters, one can employ the criterion given by equation (36) and the method provided in section 5.4.2. to verify that the other potential solutions are not viable. Based on this, one can be quite certain that the absorber performance predicted in the following section can be achieved.

6.2. ABSORBER PERFORMANCE ON $SM2^+$

The peak rotor acceleration $\|yy'\|_{ss}$ is first derived. On $SM2^+$, the absorber motions are represented by the single-mode solution given in equations (31) and (32). These solutions are incorporated in expression (15) for the rotor acceleration, the scalings in equations (12) and (13) are employed, and terms up to $\mathcal{O}(\varepsilon)$ are retained, yielding

$$\|yy'\|_{ss} \simeq \left[(2\hat{\mu}_a)^2 + \left(\frac{4\tilde{\delta}_{\xi 2}}{n} + \frac{6\hat{\delta}_{\xi 4}\bar{r}_{\eta+}^2}{n}\right)^2\right]^{1/2} \quad \text{on } SM2^+, \tag{45}$$

where $\bar{r}_{\eta+}^2$ is given by equation (31). Note that this reduces to zero in the undamped, perfectly tuned case.

The applied torque range $\bar{\tilde{F}}_\theta$ is simply set by the upper torque limit at which the absorbers hit the cusps on the $SM2^+$ branch, given by equation (37). Utilizing the scaling assumptions (11)–(13), one can obtain $\bar{\tilde{F}}_\theta$ by scaling equation (37), resulting in

$$\bar{\tilde{F}}_\theta \simeq \left[\left(\frac{2nv}{n^2+4} + \frac{96\hat{\delta}_{\xi 4}}{n^3(n^2+4)} + \frac{4\hat{\delta}_{\xi 2}}{n}\right)^2 + 4\hat{\mu}_a^2\right]^{1/2}. \tag{46}$$

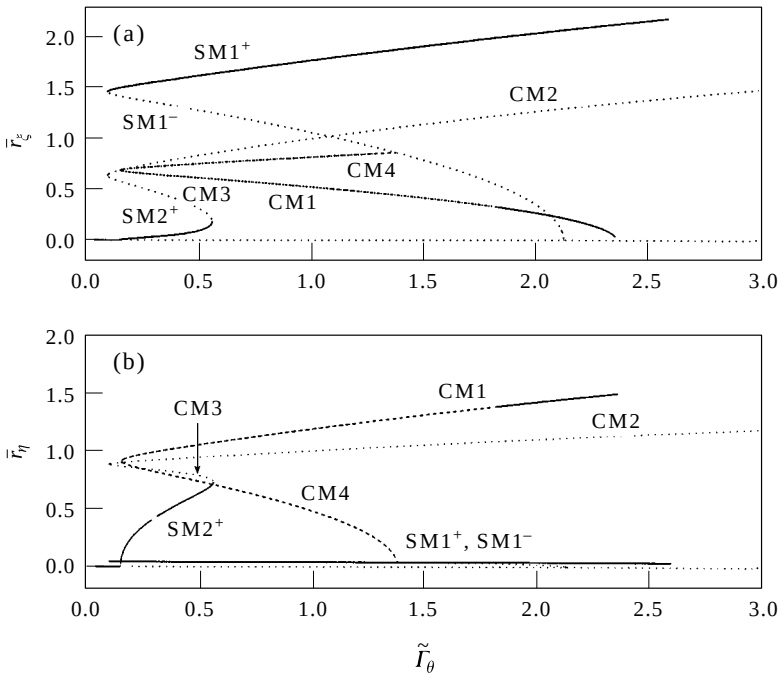

Figure 7. The response bifurcation diagram for $n = 2$, $\tilde{\mu}_a = 0{\cdot}05$, $\hat{\delta}_{\xi 2} = 0{\cdot}01$, $\hat{\delta}_{\eta 2} = 0{\cdot}01$, $\hat{\delta}_{\xi 4} = 0$ and $\hat{\delta}_{\eta 4} = 0$. The solid lines represent stable solutions and the dashed lines represent unstable solutions; (a) amplitudes of ξ; (b) amplitudes of η.

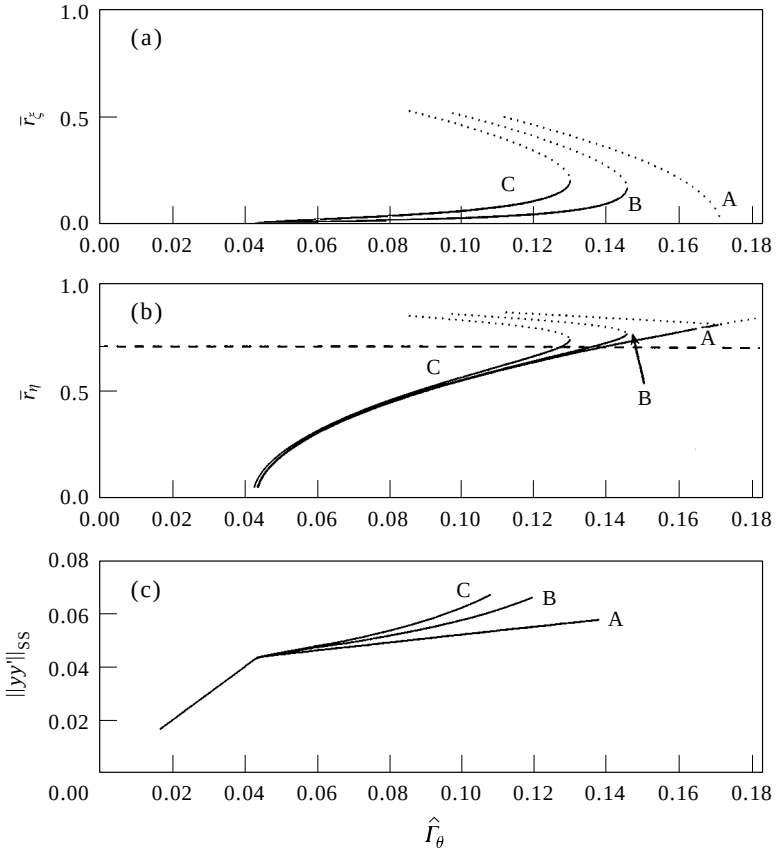

Figure 8. The response bifurcation diagram of SM2 for $n = 2$, $\hat{\mu}_a = 0{\cdot}0083$, $\hat{\delta}_{\xi 2} = 0{\cdot}02$ and $\hat{\delta}_{\xi 4} = 0{\cdot}01$, $\hat{\delta}_{\eta 4} = 0$ and various $\hat{\delta}_{\eta 2}$. (a) Amplitudes of ξ, where $\hat{\delta}_{\eta 2} = 0{\cdot}0$, $0{\cdot}01$, $0{\cdot}02$ in curves A, B, C, respectively; (b) amplitudes of η; (c) rotor accelerations.

This is the generalization of the result given in equation (10) for the ideal system, accounting for the effects of absorber damping, mistuning and imperfections. Note that this result assumes that the cusp is reached before a secondary bifurcation takes place, and this can be checked for each case by the procedure outlined in section 5.3.3.

6.3. THE EFFECTS OF IMPERFECTIONS

The effects of $\hat{\delta}_{\xi 2}$, $\hat{\delta}_{\xi 4}$, $\hat{\delta}_{\eta 2}$ and $\hat{\delta}_{\eta 4}$ are considered in turn in this section. Recall that these scaled parameters capture the effects of mistunings and imperfections associated with the second and fourth order coefficients in the path function (8).

Observing the solutions for SM2$^+$ given by equation (31), one sees that a small non-zero value of $\hat{\delta}_{\xi 4}$ does not qualitatively change system behavior since it only affects the magnitude of the coefficient c_{n4}. Based on this fact, the effects of $\hat{\delta}_{\xi 2}$ on absorber performance are first considered for the case when $\hat{\delta}_{\xi 4}$ is zero.

It is seen from equation (45) that for $\hat{\delta}_{\xi 4} = 0$, $\|yy'\|_{ss}$ depends on the parameters $\hat{\mu}_a$, n, and $\hat{\delta}_{\xi 2}$ (for $\hat{\delta}_{\xi 4} = 0$), but it is independent of the disturbing torque level and independent of the absorbers' amplitudes. This indicates that the rotor acceleration saturates after the bifurcation point, a result that is valid until $\hat{\Gamma}_\theta$ reaches $\hat{\bar{F}}_\theta$. The results for this case are shown in bifurcation diagrams for various values of $\hat{\delta}_{\xi 2}$ with $n = 2$, $\hat{\mu}_a = 0{\cdot}0083$ ($\tilde{\mu}_a = 0{\cdot}05$) and $\hat{\delta}_{\xi 4} = 0$ and are now described. (Recall that the parameter $\hat{\delta}_{\xi 2}$ controls the linear

of the absorbers.) Figures 5(a) and 5(c) show the response of $\bar{r}_\eta$ for positive and negative values of $\hat{\delta}_{\xi 2}$, respectively (recall that $\bar{r}_\xi = 0$ on the branch being considered). Figure 5(b) and 5(d) show the corresponding rotor accelerations up to the torque level $\hat{\bar{F}}_\theta$, where the absorber motions hit the cusps. It can be seen from these figures that the level of rotor acceleration is smallest for zero mistuning, case D (as expected). However, the largest torque range is obtained for the largest positive value of mistuning considered here, case A. It is also observed that the amplitudes of the absorber motions are much larger for negative values of $\hat{\delta}_{\xi 2}$ than for positive values. Furthermore, for negative values of $\hat{\delta}_{\xi 2}$, a highly undesirable subcritical bifurcation takes the system to the desired subharmonic solution as the torque level is increased. Therefore, in order to ensure a large torque range, to avoid jump behaviors, and to keep $\|yy'\|_{ss}$ small, it is suggested that the absorber paths be designed such that $\hat{\delta}_{\xi 2}$ is very small and positive. The selection of a specific value for $\hat{\delta}_{\xi 2}$ will depend on the criteria at hand, as tradeoffs between the torque range and torsional vibration amplitudes can be made, as well as on the level of uncertainties in the paths due to uncontrollable effects.

The effects of nonzero $\hat{\delta}_{\xi 4}$ on absorber performance are considered next. Throughout this discussion it is assumed that $\hat{\delta}_{\xi 2}$ is positive and small. Utilizing equations (45) and (46), bifurcation diagrams are generated for various values of $\hat{\delta}_{\xi 4}$. An example for $n = 2$, $\hat{\mu}_a = 0{\cdot}0083$ and $\hat{\delta}_{\xi 2} = 0{\cdot}02$ is shown in Figure 6. By comparing the responses with positive and negative values of $\hat{\delta}_{\xi 4}$, it is seen that negative values offer better performance in terms

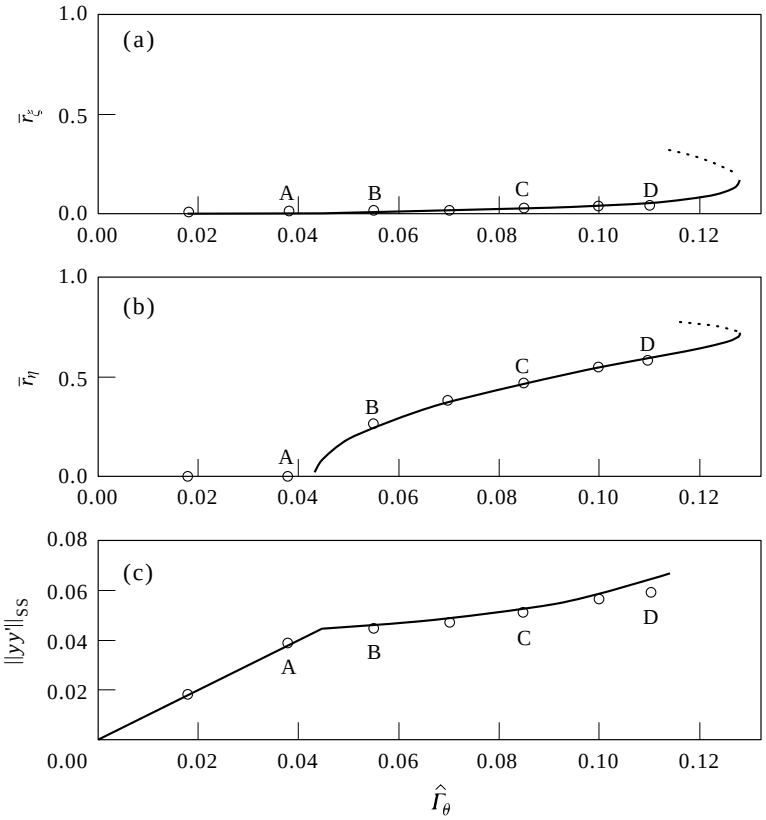

Figure 9. The simulated and analytical responses of SM2 for $n = 2$, $\hat{\mu}_a = 0{\cdot}0083$, $\hat{\delta}_{\xi 2} = 0{\cdot}02$, $\hat{\delta}_{\xi 4} = 0{\cdot}01$, $\hat{\delta}_{\eta 2} = 0{\cdot}005$ and $\hat{\delta}_{\eta 4} = 0{\cdot}005$. (a) Amplitudes of ξ; (b) amplitudes of η; (c) rotor accelerations.

of the rotor acceleration, but they also reduce the applied torque range. On the other hand, although positive values of $\hat{\delta}_{\xi 4}$ lead to a larger torque range, they cause an increase in the level of rotor acceleration.

The results given above are based on scaling assumption (25), which says that the differences between the two absorber paths are smaller than the general level of imperfections. This condition is now relaxed in order to consider the effects of nonzero, small $\hat{\delta}_{\eta}$s. Due to the complexity of the resulting averaged equations, bifurcation diagrams can only be generated numerically, in this case using AUTO. The effects of the imperfection parameter $\hat{\delta}_{\eta 2}$ are considered first. Figure 7 shows the bifurcation diagram with the same system parameters used in Figure 2, but with $\hat{\delta}_{\eta 2} = 0{\cdot}01$ and $\hat{\delta}_{\eta 4} = 0$. Comparing Figures 2 and 7, it is seen that they are qualitatively the same, except that the zero amplitude parts of the solutions in the two single-mode responses are replaced by nonzero, but very small, amplitudes. (Note that the solutions denoted by $SM1^+$, $SM1^-$ and $SM2^+$ in the figure are labelled so for convenience and for comparison purposes only, since they are in fact coupled-mode solutions in this case.) Figure 8 shows the solutions for $\bar{r}_{\xi}$, $\bar{r}_{\eta}$, and the corresponding rotor accelerations on the branch $SM2^+$ for $\hat{\delta}_{\xi 2} = 0{\cdot}02$, $\hat{\delta}_{\xi 4} = 0{\cdot}01$, $\hat{\delta}_{\eta 4} = 0$ and various values of $\hat{\delta}_{\eta 2}$. It is seen that the existence of a nonzero component of $\bar{r}_{\xi}$ decreases the applicable torque range and increases the rotor acceleration as the magnitude of $\hat{\delta}_{\eta 2}$ becomes larger. Both effects deteriorate absorber performance. In addition, the parameter $\hat{\delta}_{\eta 4}$ is found to have the same detrimental effects on the system behavior as $\hat{\delta}_{\eta 2}$. Therefore, both of these parameters should be kept as small as possible.

6.4. DESIGN GUIDELINES

In summary, the above results indicate that the following general guidelines be followed when designing the paths for a subharmonic absorber system:

- The absorber paths should be kept as identical as possible.
- The nonlinear imperfection parameter $\hat{\delta}_{\xi 4}$ should be made as small as possible.
- The linear mistuning parameter $\hat{\delta}_{\xi 2}$ should be selected to be small and positive, at a level that will dominate other imperfection uncertainties.

In summary, identical, half-order epicycloidal paths that are very slightly overtuned should be used in order to achieve robust performance.

6.5. SIMULATION RESULTS

Numerical simulations for the equations of motion (3) are carried out in order to verify the system dynamics as predicted by the averaged equations. The system parameters used throughout this section are $v = 0{\cdot}166$ and $n = 2$, values taked from the study of a 2·5-liter, in-line, four stroke, four cylinder engine by Denman [7]. The damping coefficients are taken to be $\hat{\mu}_0 = 0{\cdot}05$ and $\hat{\mu}_a = 0{\cdot}0083$ ($\tilde{\mu}_a = 0{\cdot}05$). The following truncated absorber path formulation, expressed in terms of the $\hat{\delta}$s, is employed; equation (8) given by

$$x_i(s_i; \hat{\delta}_{ij}) = 1 - \hat{\delta}_{i1} s_i - \left[\left(\frac{n}{2}\right)^2 + \hat{\delta}_{i2}\right] s_i^2 - \hat{\delta}_{i3} s_i^3 - \hat{\delta}_{i4} s_i^4, \qquad i = 1, 2. \tag{47}$$

Higher-order imperfections are not included here, since it is evident that they will not contribute to the first-order nonlinear resonant responses. In all cases the coefficients of odd powers of s, $\hat{\delta}_{\xi 1}$, $\hat{\delta}_{\eta 1}$, $\hat{\delta}_{\xi 3}$ and $\hat{\delta}_{\eta 3}$ are assumed to be small. The simulations show that these $\hat{\delta}$s have virtually no effect on the system response, as predicted by the analysis. Overall, excellent consistency is found between the analytical results derived from the non-truncated averaged equations (22) and the simulations.

A representative case is chosen to demonstrate the simulation results and their comparison with the analysis. Imperfection parameters for this case are taken to be

$$\hat{\delta}_{\xi 1} = 0{\cdot}01, \quad \hat{\delta}_{\eta 1} = 0{\cdot}01, \quad \hat{\delta}_{\xi 2} = 0{\cdot}02, \quad \hat{\delta}_{\eta 2} = 0{\cdot}005,$$
$$\hat{\delta}_{\xi 3} = 0{\cdot}01, \quad \hat{\delta}_{\eta 3} = 0{\cdot}01, \quad \hat{\delta}_{\xi 4} = 0{\cdot}01, \quad \hat{\delta}_{\eta 4} = 0{\cdot}005. \tag{48}$$

Here the linear frequency mistuning for the two absorbers is 2% (for $n = 2$) with a deviation between absorbers of 0·5% represented by $\hat{\delta}_{\eta 2} = 0{\cdot}005$. A small, positive $\hat{\delta}_{\xi 4} = 0{\cdot}01$ is chosen, which enlarges the range of the disturbing torque but also increases rotor acceleration amplitudes. In order to demonstrate the influence of different nonlinear characteristics between the two paths, a small deviation represented by $\hat{\delta}_{\eta 4} = 0{\cdot}005$ is chosen. The bifurcation diagram using this set of values is shown in Figure 9. The solid lines represent the absorber amplitude solutions, as computed by AUTO using the non-truncated averaged equations (22), and the corresponding rotor acceleration, which is calculated by the $\mathcal{O}(\varepsilon)$ term of $yy'(\theta)$ given in equation (15). The circles are the results obtained from simulations, after allowing the system to settle into its steady-state response. It is seen from this figure that the averaged equations (22) offer a very satisfactory prediction of the system dynamics, even for this moderate value of the perturbation parameter, $\varepsilon = 0{\cdot}166$.

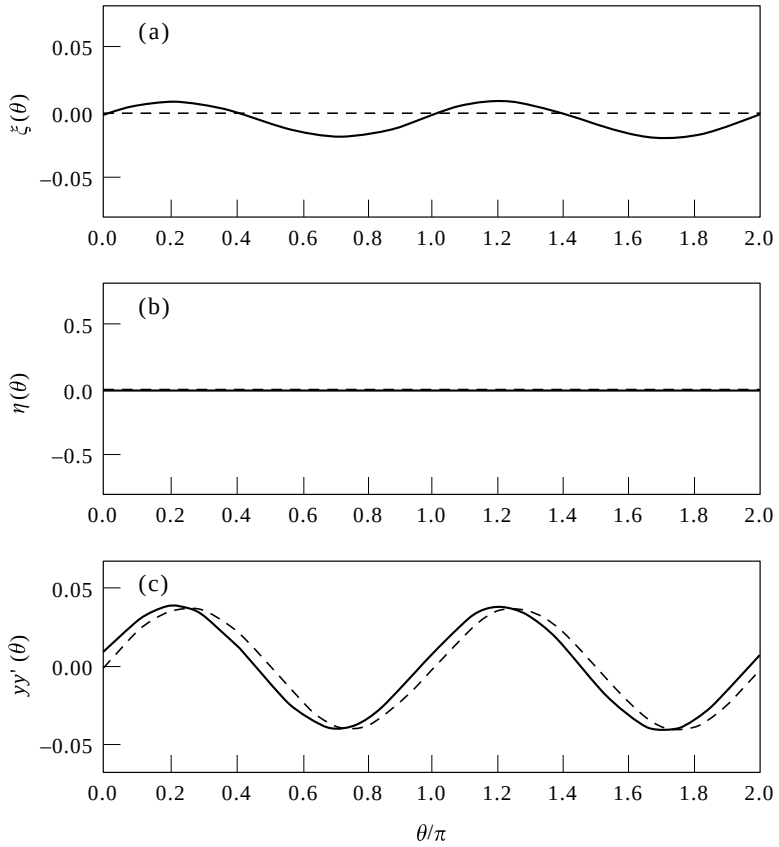

Fig. 10. *Caption on p.* 1094

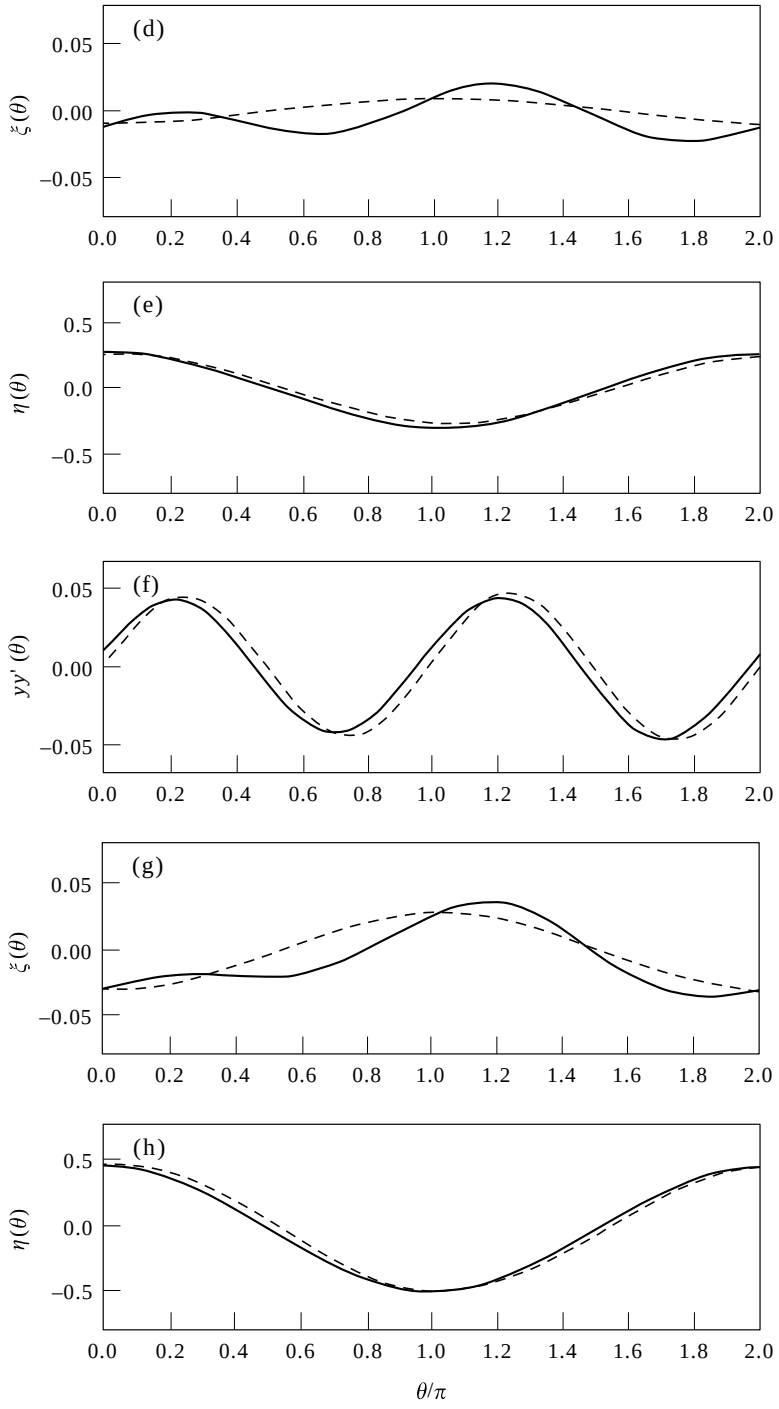

Fig. 10. *Caption on p*. 1094.

Figure 10 shows the system responses and the angular accelerations of the rotor at points A, B, C, and D indicated in Figure 9. Solid lines represent the simulated responses while the dashed lines represent the responses predicted by the nontruncated averaged equations

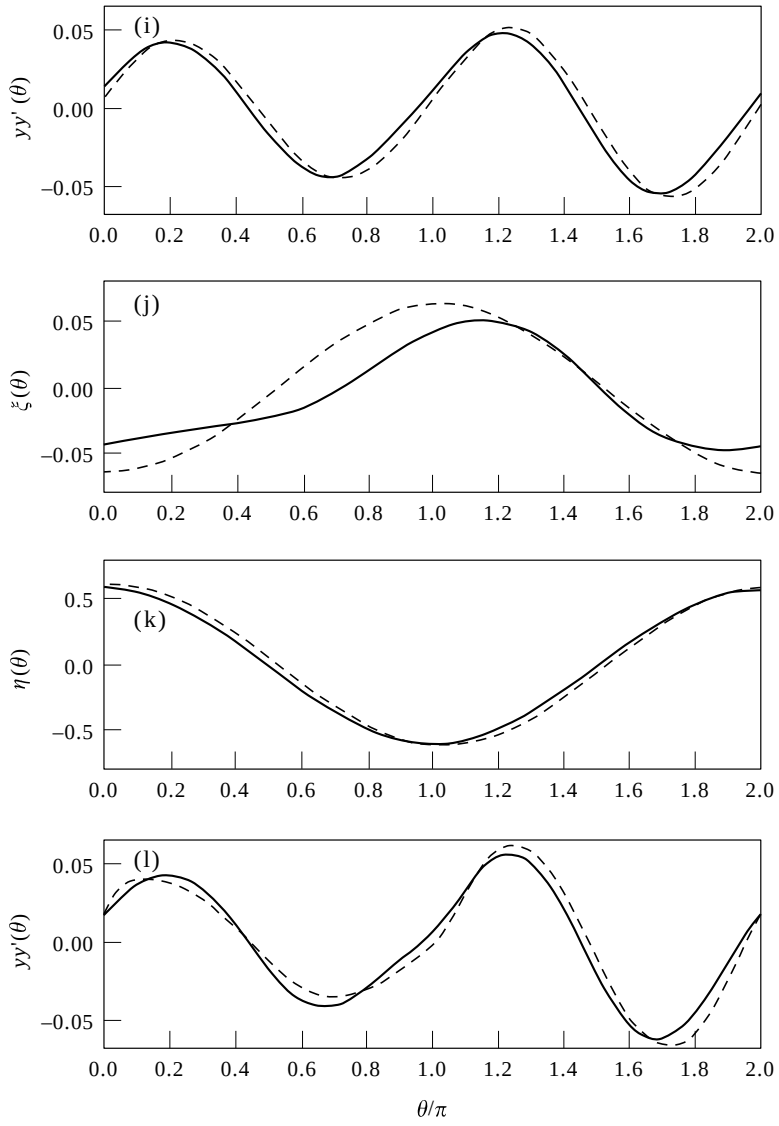

Figure 10. The absorber responses and rotor accelerations for $\hat{\Gamma}_\theta = 0{\cdot}038, 0{\cdot}055, 0{\cdot}085, 0{\cdot}11$, in cases A, B, C, D respectively. These cases correspond to points A, B, C and D in Figure 9. (a, d, g, j) Amplitudes of ξ; (b, e, h, k) amplitudes of η; (c, f, i, l) rotor accelerations.

(22). Note that the scale used to depict the $\xi(\theta)$ response in Figure 10(a, d, g, j) is expanded for greater clarity. It is seen from subfigures (b, c, e, f, h, i, k, l) that the approximations obtained from averaging for the crucial response variables $yy'(\theta)$ and $\eta(\theta)$ are very accurate.

At point A, the simulations show that the absorber motions are dictated by the non-resonant responses, i.e. the absorbers respond in a synchronized manner at the frequency of the disturbing torque (essentially, the linear system response). For this case the averaged equations predict zero resonant responses for both $\xi(\theta)$ and $\eta(\theta)$. At point B, as predicted by the averaged equations, a subharmonic resonant response with a frequency half that of the disturbing torque has appeared. This response possesses a

non-zero response in the difference coordinate $\eta(\theta)$ and a very small response in the sum coordinate $\xi(\theta)$. Figure 10(d, e) shows that the simulated $\eta(\theta)$ matches well with the analysis, while the simulated $\xi(\theta)$ is approximately a superposition of the non-resonant response shown in Figure 10(a) (which is not predicted by the analysis) and the resonant response (which is predicted). In this case, the absorber motions are dominated by the out-of-phase component $\eta(\theta)$. From (g) to (j), as $\hat{\Gamma}_\theta$ is increased, the response of $\xi(\theta)$ grows and begins to influence the rotor acceleration. In addition, higher harmonics begin to have a more significant effect on the response.

Using the simulations, one also finds consistency between the predicted and simulated torque ranges. This follows since $\eta(\theta)$ is well approximated by the analytical results, and in the range of large torque amplitudes the absorber motion is dominated by this component.

7. CONCLUSIONS AND DIRECTIONS FOR FUTURE WORK

The performance of a pair of subharmonic absorbers as proposed by reference [15] has been re-assessed by incorporating imperfections into the absorber paths. Based onk approximate solutions obtained by a particular scaling of the sytem parameters and applying the method of averaging, it is found that the imperfections entering the path function at even orders of the path variable s have a strong effect on the desired resonant responses of the system. It is also found that differences between the two paths of the absorbers have a generally deleterious effect on system performance. On the other hand, imperfections that are identical to the two paths can be used to trade off between the operating range of the system and the level of torsional vibration and, more importantly, it may be possible to use these to intentionally dominate the potentially detrimental effects of uncertainties in the absorber path.

This work only considered a rotating system with a single pair of subharmonic absorbers. In practice, one may need to station several absorber masses along and around the axis of rotation. These multi-mass arrangements are also used for balancing and/or due to restricted space around the rotor. In many cases, these absorbers are of identical mass and have identical path tuning. Recent studies in which the absorber paths are tuned to the order of the disturbing torque (the usual, linear tuning) have shown that multi-absorber systems can exhibit a qualitatively different absorber performance than their idealized counterparts composed of a single mass [13, 14]. This discrepancy arises due to a dynamic bifurcation of the system response that depends on the number of absorber masses employed. In a similar investigation, the authors have shown that the design guidelines presented here will also ensure that systems of identical, multiple, subharmonic absorber pairs will behave as predicted, and as desired [21]. Detailed results from that study will be presented in a forthcoming paper.

ACKNOWLEDGMENTS

The previous investigations of Dr Cheng-Tang Lee have been crucial for this study, and the authors are grateful to him for his ground-breaking work in this area. This research was supported in part by a grant from the National Science Foundation.

REFERENCES

1. B. C. Carter 1929 *British Patent NO*. 337, 446.
2. W. Ker Wilson 1968 *Practical Solution of Torsional Vibration Problems*. London: Chapman & Hall. 3rd edn, Chap. XXX, Vol. IV.

3. D. E. Newland 1964 *ASME Journal of Engineering for Industry* **86**, 257–263. Nonlinear aspects of the performance of centrifugal pendulum vibration absorbers.
4. M. Sharif-Bakhtiar and S. W. Shaw 1992 *ASME Journal of Vibration and Acoustics* **114**, 305–311. Effects of nonlinearities and damping on the dynamic response of a centrifugal pendulum absorber.
5. J. P. Den Hartog 1938 In *Stephen Timoshenko 60th Anniversary Volume*. New York: Macmillan. Tuned pendulums as torsional vibration eliminators, 17–26.
6. J. F. Madden 1980 *United States Patent No*. 4218187. Constant frequency bifilar vibration absorber.
7. H. H. Denman 1992 *Journal of Sound and Vibration* **159**, 251–277. Tautochronic bifilar pendulum torsion absorbers for reciprocating engines.
8. V. J. Borowski, H. H. Denman, D. L. Cronin, S. W. Shaw, J. P. Hanisko, L. T. Brooks, D. A. Milulec, W. B. Crum and M. P. Anderson 1991 *SAE Technical Paper Series* 911876. Reducing vibration of reciprocating engines with crankshaft pendulum vibration absorbers.
9. S. W. Shaw and C.-T. Lee 1995 In *Smart Structures, Nonlinear Vibration, and Control*, A. Guran and D. J. Inman, eds. Englewood Cliffs, NJ: Prentice-Hall. On the nonlinear dynamics of centrifugal pendulum vibration absorbers, 247–309.
10. S. W. Shaw, V. K. Garg and C.-P. Chao 1997 *SAE Noise and Vibration Conference and Exposition*. Attenuation of engine torsional vibrations using tuned pendulum absorbers, Vol. 2, 713–722.
11. C.-T. Lee and S. W. Shaw 1994 In *Nonlinear and Stochastic Dynamics*, *ASME WAM*. A comparative study of nonlinear centrifugal pendulum vibration absorbers, Vol. AMD-Vol. 192/DE-Vol. 78, 91–98.
12. C.-T. Lee and S. W. Shaw 1997 *Journal of Sound and Vibration* **203**, 731–743. Nonlinear dynamic response of paired centrifugal pendulum vibration absorbers.
13. C.-P. Chao, S. W. Shaw and C.-T. Lee 1997 *ASME Journal of Applied Mechanics* **64**, 149–156. Stability of the unison response for a rotating system with multiple centrifugal pendulum vibration absorbers.
14. C.-P. Chao, C.-T. Lee and S. W. Shaw 1997 *Journal of Sound and Vibration* **204**, 769–794. Nonlinear-unison dynamics of multiple centrifugal pendulum vibration absorbers.
15. C.-T. Lee, S. W. Shaw and V. T. Coppola 1997 *ASME Journal of Vibration and Acoustics* **119**, 590–595. A subharmonic vibration absorber for rotating machinery.
16. X. L. Yang and P. R. Sethna 1991 *International Journal of Non-Linear Mechanics* **26**, 199-220. Local and global bifurcations in parametrically excited vibrations of nearly square plates.
17. J. A. Murdock 1991 *Perturbations*: *Theory and Methods*. New York: Wiley.
18. A. K. Bajaj, P. Davies and C. S. I. 1995 In *Nonlinear Dynamics and Stochastic Mechanics*, W. Kliemann and N. Sri Namachchivaya, eds. Boca Raton, FL: CRC Press. On internal resonances in mechanical systems, 69–94.
19. S. T. Ariaratnam and N. Sri Namachchivaya 1986 *Journal of Structural Mechanics* **114**, 153–175. Periodically perturbed nonlinear gyroscopic systems.
20. E. Doedel 1985 *Auto*: *software for Continuation and Bifurcation Problems in Ordinary Differential Equations*. Department of Applied Mathematics, California Institute of Technology, Pasadena, CA.
21. C.-P. Chao 1997 *Ph.D. thesis*, *Department of Mechanical Engineering*, *Michigan State University*, *East Lansing*. The performance of multiple pendulum vibration absorbers applied to rotating systems.

APPENDIX A: AVERAGED EQUATIONS IN CARTESIAN COORDINATES

The truncated, averaged equations in Cartesian coordinates are given by

$$\frac{\mathrm{d}A_\xi}{\mathrm{d}\tilde{\theta}} = \frac{-1}{2}\,\tilde{\mu}_a A_\xi + \left(\frac{\tilde{\delta}_{\xi 2}}{n} + \frac{n}{4}\right)B_\xi + \frac{\tilde{\delta}_{\eta 2}}{n}\,B_\eta + \frac{1}{4}\,\tilde{\Gamma}_\theta B_\xi$$

$$- c_{n2}B_\xi(A_\xi^2 + B_\xi^2) + c_{n5}A_\xi A_\eta B_\eta - c_{n6}B_\xi A_\eta^2 + c_{n7}B_\xi B_\eta^2$$

$$+ \frac{3\tilde{\delta}_{\eta 4}}{2n}\,(A_\eta^2 B_\eta + A_\xi^2 B_\eta + 3B_\eta B_\xi^2 + B_\eta^3 + 2A_\eta A_\xi B_\xi), \tag{A1a}$$

$$\frac{\mathrm{d}B_\xi}{\mathrm{d}\hat{\theta}} = \frac{-1}{2}\,\tilde{\mu}_a B_\xi - \left(\frac{\tilde{\delta}_{\xi 2}}{n} + \frac{n}{4}\right)A_\xi - \frac{\tilde{\delta}_{\eta 2}}{n}\,A_\eta + \frac{1}{4}\,\tilde{\Gamma}_\theta A_\xi$$

$$+ c_{n2}A_\xi(A_\xi^2 + B_\xi^2) - c_{n5}B_\xi A_\eta B_\eta + c_{n6}A_\xi B_\eta^2 - c_{n7}A_\xi A_\eta^2,$$

$$- \frac{3\tilde{\delta}_{\eta 4}}{2n}\,(B_\eta^2 A_\eta + B_\xi^2 A_\eta + 3A_\eta A_\xi^2 + A_\eta^3 + 2B_\eta A_\xi B_\xi), \tag{A1b}$$

$$\frac{\mathrm{d}A_\eta}{\mathrm{d}\hat{\theta}} = \frac{-1}{2}\,\tilde{\mu}_a A_\eta + \frac{\tilde{\delta}_{\xi 2}}{n}\,B_\eta + \frac{\tilde{\delta}_{\eta 2}}{n}\,B_\xi + \frac{1}{4}\,\tilde{\Gamma}_\theta B_\eta$$

$$+ c_{n4}B_\eta(A_\eta^2 + B_\eta^2) + c_{n5}A_\eta A_\xi B_\xi - c_{n6}B_\eta A_\xi^2 + c_{n7}B_\eta B_\xi^2,$$

$$+ \frac{3\tilde{\delta}_{\eta 4}}{2n}\,(A_\xi^2 B_\xi + A_\eta^2 B_\xi + 3B_\xi B_\eta^2 + B_\xi^3 + 2A_\xi B_\eta A_\eta), \tag{A1c}$$

$$\frac{\mathrm{d}B_\eta}{\mathrm{d}\hat{\theta}} = \frac{-1}{2}\,\tilde{\mu}_a B_\eta - \frac{\tilde{\delta}_{\eta 2}}{n}\,A_\xi - \frac{\tilde{\delta}_{\xi 2}}{n}\,A_\eta + \frac{1}{4}\,\tilde{\Gamma}_\theta A_\eta$$

$$- c_{n4}A_\eta(A_\eta^2 + B_\eta^2) - c_{n5}A_\xi B_\xi B_\eta + c_{n6}A_\eta B_\xi^2 - c_{n7}A_\eta A_\xi^2$$

$$- \frac{3\tilde{\delta}_{\eta 4}}{2n}\,(B_\xi^2 A_\xi + B_\eta^2 A_\xi + 3A_\xi A_\eta^2 + A_\xi^3 + 2B_\xi A_\eta B_\eta). \tag{A1d}$$

where

$$c_{n5} = \frac{4n^3 - n^5}{128} + \frac{3\tilde{\delta}_{\xi 4}}{n}, \qquad c_{n6} = \frac{12n^3 + n^5}{256} - \frac{3\tilde{\delta}_{\xi 4}}{2n} \qquad \text{and} \qquad c_{n7} = \frac{-4n^3 - 3n^5}{256} + \frac{3\tilde{\delta}_{\xi 4}}{2n}.$$

Applying the assumption (25), the above equations become

$$\frac{\mathrm{d}A_\xi}{\mathrm{d}\hat{\theta}} = \frac{-1}{2}\,\tilde{\mu}_a A_\xi + \left(\frac{\tilde{\delta}_{\xi 2}}{n} + \frac{n}{4}\right)B_\xi + \frac{1}{4}\,\tilde{\Gamma}_\theta B_\xi - c_{n2}B_\xi(A_\xi^2 + B_\xi^2)$$

$$+ c_{n5}A_\xi A_\eta B_\eta - c_{n6}B_\xi A_\eta^2 + c_{n7}B_\xi B_\eta^2, \tag{A2a}$$

$$\frac{\mathrm{d}B_\xi}{\mathrm{d}\hat{\theta}} = \frac{-1}{2}\,\tilde{\mu}_a B_\xi - \left(\frac{\tilde{\delta}_{\xi 2}}{n} + \frac{n}{4}\right)A_\xi + \frac{1}{4}\,\tilde{\Gamma}_\theta A_\xi + c_{n2}A_\xi(A_\xi^2 + B_\xi^2)$$

$$- c_{n5}B_\xi A_\eta B_\eta + c_{n6}A_\xi B_\eta^2 - c_{n7}A_\xi A_\eta^2, \tag{A2b}$$

$$\frac{\mathrm{d}A_\eta}{\mathrm{d}\hat{\theta}} = \frac{-1}{2}\,\tilde{\mu}_a A_\eta + \frac{\tilde{\delta}_{\xi 2}}{n}\,B_\eta + \frac{1}{4}\,\tilde{\Gamma}_\theta B_\eta + c_{n4}B_\eta(A_\eta^2 + B_\eta^2)$$

$$+ c_{n5}A_\eta A_\xi B_\xi - c_{n6}B_\eta A_\xi^2 + c_{n7}B_\eta B_\xi^2, \tag{A2c}$$

$$\frac{\mathrm{d}B_\eta}{\mathrm{d}\hat{\theta}} = \frac{-1}{2}\,\tilde{\mu}_a B_\eta - \frac{\tilde{\delta}_{\xi 2}}{n}\,A_\eta + \frac{1}{4}\,\tilde{\Gamma}_\theta A_\eta - c_{n4}A_\eta(A_\eta^2 + B_\eta^2)$$

$$- c_{n5}A_\xi B_\xi B_\eta + c_{n6}A_\eta B_\xi^2 - c_{n7}A_\eta A_\xi^2. \tag{A2d}$$

APPENDIX B: STABILITY OF SOLUTIONS ON SM1$^+$

Incorporating the SM1$^+$ solutions given by equation (31) into the sub-block matrix B in the corresponding Jacobian, one can obtain the determinant of B, D_{B1+}. It is given by

$$\begin{aligned} D_{B1+} = & -\frac{\tilde{\Gamma}_\theta^2}{16} + \frac{\tilde{\mu}_a^2}{4} + \frac{\tilde{\delta}_{\xi 2}^2}{n^2} \\ & - \left(\frac{c_{n6} + c_{n7}}{16 c_{n2}}\right)(\tilde{\Gamma}_\theta^2 - 4\tilde{\mu}_a^2)^{1/2}\left[(\tilde{\Gamma}_\theta^2 - 4\tilde{\mu}_a^2)^{1/2} + \frac{4\tilde{\delta}_{\xi 2}}{n} + n\right] \\ & + \left(\frac{c_{n6}^2 - 6c_{n6}c_{n7} + c_{n7}^2 - c_{n5}^2}{128 c_{n2}^2}\right)\left[(\tilde{\Gamma}_\theta^2 - 4\tilde{\mu}_a^2)^{1/2} + \frac{4\tilde{\delta}_{\xi 2}}{n} + n\right]^2 \\ & + \left(\frac{c_{n5}^2 - c_{n6}^2 - 2c_{n6}c_{n7} - c_{n7}^2}{128 c_{n2}^2}\right)\left(1 - \frac{8\tilde{\mu}_a}{\tilde{\Gamma}_\theta^2}\right)\left[(\tilde{\Gamma}_\theta^2 - 4\tilde{\mu}_a^2)^{1/2} + \frac{4\tilde{\delta}_{\xi 2}}{n} + n\right]^2 \\ & - \left[\frac{(c_{n6} - c_{n7})\tilde{\delta}_{\xi 2}}{4 c_{n2} n}\right]\left[(\tilde{\Gamma}_\theta^2 - 4\tilde{\mu}_a^2)^{1/2} + \frac{4\tilde{\delta}_{\xi 2}}{n} + n\right]. \end{aligned}$$

APPENDIX C: STABILITY OF SOLUTIONS ON SM2$^+$

Incorporating the SM2$^+$ solutions given by equation (32) into the sub-block matrix A in the corresponding Jacobian, one can obtain the determinant of A, D_{A2+}. It is given by

$$\begin{aligned} D_{A2+} = & \frac{\tilde{\delta}_{\xi 2}}{2} - \frac{\tilde{\Gamma}_\theta^2}{16} + \frac{\tilde{\mu}_a^2}{4} + \frac{\tilde{\delta}_{\xi 2}^2}{n^2} + \frac{n^2}{16} + \left(\frac{c_{n6} + c_{n7}}{16 c_{n4}}\right)(\tilde{\Gamma}_\theta^2 - 4\tilde{\mu}_a^2)^{1/2}\left[(\tilde{\Gamma}_\theta^2 - 4\tilde{\mu}_a^2)^{1/2} - \frac{4\tilde{\delta}_{\xi 2}}{n}\right] \\ & + \left(\frac{c_{n6}^2 - 6c_{n6}c_{n7} + c_{n7}^2 - c_{n5}^2}{128 c_{n4}^2}\right)\left[(\tilde{\Gamma}_\theta^2 - 4\tilde{\mu}_a^2)^{1/2} - \frac{4\tilde{\delta}_{\xi 2}}{n}\right]^2 \\ & + \left(\frac{c_{n5}^2 - c_{n6}^2 - 2c_{n6}c_{n7} - c_{n7}^2}{128 c_{n4}^2}\right)\left(1 - \frac{8\tilde{\mu}_a}{\tilde{\Gamma}_\theta^2}\right)\left[(\tilde{\Gamma}_\theta^2 - 4\tilde{\mu}_a^2)^{1/2} - \frac{4\tilde{\delta}_{\xi 2}}{n}\right]^2 \\ & - \left(\frac{c_{n6} - c_{n7}}{4 c_{n4}}\right)\left(\frac{\tilde{\delta}_{\xi 2}}{n} + \frac{n}{4}\right)\left[(\tilde{\Gamma}_\theta^2 - 4\tilde{\mu}_a^2)^{1/2} - \frac{4\tilde{\delta}_{\xi 2}}{n}\right]. \end{aligned}$$

APPENDIX D: THE NUMERICAL ALGORITHM FOR COUPLED-MODE SOLUTIONS

The coupled-mode solutions are numerically computed by the following steps.

(1) Compute the possible sets of solutions for $\bar{r}_\xi$ and $\bar{r}_\eta$ using the polynomial (43)

(2) For each set of solutions for $\bar{r}_\xi$ and $\bar{r}_\eta$, calculate the corresponding applied torque amplitude by combining equations (40a) and (40c), which yields

$$2\tilde{\mu}_a(\bar{r}_\eta^2 + \bar{r}_\xi^2) + \tilde{\Gamma}_\theta(\bar{r}_\eta^2 \sin 2\bar{\varphi}_\eta + \bar{r}_\xi^2 \sin 2\bar{\varphi}_\xi) = 0. \tag{D1}$$

The dependence of equation (D1) on $\bar{\varphi}_\eta$ and $\bar{\varphi}_\xi$ is then eliminated by using equations (42a) and (42b). This results in a nonlinear algebraic equation which can be used to solve for $\tilde{\Gamma}_\theta$ for given values of $\bar{r}_\xi$ and $\bar{r}_\eta$. Thus, one can find the values of $\bar{r}_\xi$ and $\bar{r}_\eta$ for a given $\tilde{\Gamma}_\theta$ in a reverse manner. Using equations (42a) and (42b) again, one can determine the corresponding values of $\bar{\varphi}_\xi$ and $\bar{\varphi}_\eta$.